Published in final edited form as:

Nature. 2020 October ; 586(7829): 429–433. doi:10.1038/s41586-020-2719-5.

STING cyclic dinucleotide sensing originated in bacteria

Benjamin R. Morehouse[1,2], **Apurva A. Govande**[1,2], **Adi Millman**[3], **Alexander F.A. Keszei**[4], **Brianna Lowey**[1,2], **Gal Ofir**[3], **Sichen Shao**[4], **Rotem Sorek**[3], **Philip J. Kranzusch**[1,2,5,*]

[1]Department of Microbiology, Harvard Medical School, Boston, MA 02115, USA

[2]Department of Cancer Immunology and Virology, Dana-Farber Cancer Institute, Boston, MA 02115, USA

[3]Department of Molecular Genetics, Weizmann Institute of Science, Rehovot 76100, Israel

[4]Department of Cell Biology, Harvard Medical School, Boston, MA 02115, USA

[5]Parker Institute for Cancer Immunotherapy at Dana-Farber Cancer Institute, Boston, MA 02115, USA

Abstract

Stimulator of interferon genes (STING) is a receptor in human cells that senses foreign cyclic dinucleotides released during bacterial infection and endogenous cyclic GMP–AMP signaling during viral infection and antitumor immunity[1–5]. STING shares no structural homology with other known signaling proteins[6–9], limiting functional analysis and preventing explanation for the origin of cyclic dinucleotide signaling in mammalian innate immunity. Here we discover functional STING homologues encoded within prokaryotic defense islands and reveal a conserved mechanism of signal activation. Crystal structures of bacterial STING define a minimal homodimeric scaffold that selectively responds to c-di-GMP synthesized by a neighboring cGAS/DncV-like nucleotidyltransferase (CD-NTase) enzyme. Bacterial STING domains couple cyclic dinucleotide recognition with protein filament formation to drive TIR effector domain oligomerization and rapid NAD^+ cleavage. We reconstruct the evolutionary events following acquisition of STING into metazoan innate immunity and determine the structure of a full-length TIR-STING fusion from the Pacific oyster *C. gigas*. Comparative structural analysis demonstrates how metazoan-specific additions to the core STING scaffold enabled a switch from direct effector function to regulation of antiviral transcription. Together, our results explain the mechanism of

*Correspondence: philip_kranzusch@dfci.harvard.edu.

Author Contributions: Experiments were designed and conceived by B.R.M., R.S., and P.J.K. Structural and biochemical experiments were performed by B.R.M. with assistance from A.A.G. and P.J.K. NAD^+ cleavage assays were performed by A.A.G. and B.R.M. Gene identification and phylogenetic analysis were performed by A.M. and R.S. Electron microscopy experiments and analysis were conducted by A.F.A.K. and S.S. STING oligomerization analysis was performed by B.L. and B.R.M. STING toxicity analysis was performed by G.O. and R.S. The manuscript was written by B.R.M. and P.J.K. All authors contributed to editing the manuscript and support the conclusions.

Author Information: The authors have no competing financial interests to declare. Correspondence and requests for materials should be addressed to P.J.K.

Additional information

Supplementary information is available for this paper at.

STING-dependent signaling and reveal conservation of a functional cGAS-STING pathway in prokaryotic bacteriophage defense.

Bioinformatic analysis of prokaryotic bacteriophage defense islands revealed a group of divergent genes encoding the first candidate proteins outside of metazoan innate immunity with predicted homology to STING (Extended Data Figure 1a)[10]. To understand a potential role for STING in bacterial signaling, we determined 1.8 Å and 2.8 Å crystal structures of candidate homologues from *Flavobacteriaceae sp.* (IMG Gene ID 2624319773) and *Capnocytophaga granulosa* (IMG Gene ID 2541326748) (Supplementary Table 1). The bacterial structures exhibit clear homology to the human STING cyclic dinucleotide binding domain and confirm this subset of defense island proteins as novel prokaryotic members of the STING family of receptors (Figure 1a). *Flavobacteriaceae sp.* STING (*Fs*STING) and *Capnocytophaga granulosa* STING (*Cg*STING) adopt a canonical V-shaped, homodimeric architecture with a hydrophobic α-helix stem similar to that observed in all structures of metazoan STING proteins (Figure 1b)[6–9]. We determined the *Fs*STING structure in complex with 3′–5′ / 3′–5′ cyclic GMP–AMP (3′,3′-cGAMP), confirming bacterial STINGs are functional cyclic dinucleotide receptors (Figure 1a). Alignment of the *Fs*STING–3′,3′-cGAMP complex with apo *Cg*STING reveals that cyclic dinucleotide binding induces rotation of the monomeric domains and results in closure of β-strands 2 and 3 to form a lid that seals a central cyclic dinucleotide binding pocket (Figure 1a; Extended Data Figure 1b–d). Although the overall architecture is conserved with metazoan STING, bacterial STING proteins are 20% smaller and strikingly compact. Metazoan insertions into the core bacterial STING fold include an extension within the β-strand lid domain, addition of a terminal α-helix required for induction of autophagy, and an unstructured C-terminal tail containing motifs required for kinase and transcription factor recruitment in vertebrates (Figure 1b)[11–14].

We analyzed bacterial STING sequences and found that 84% are encoded in Cyclic Oligonucleotide-Based Signaling System (CBASS) immunity operons (Figure 2a)[10]. Similar to cGAS-dependent sensing of viral replication in human cells[4,5], CBASS immunity relies on activation of a CD-NTase enzyme to initiate a second messenger-dependent antiviral effector response[10,15,16]. We cloned the adjacent *Flavobacteriaceae sp.* CD-NTase *CdnE* (CD-NTase in clade E) and observed that *Fs*CdnE specifically synthesizes the cyclic dinucleotide c-di-GMP (Figure 2b)[15]. *Fs*CdnE c-di-GMP synthesis is constitutively active *in vitro*, in agreement with an emerging model where CBASS immune systems may function through inhibitory molecules that repress CD-NTase activation in the absence of phage infection[10,15–17]. We confirmed the exclusive production of c-di-GMP by CdnE enzymes encoded within three additional divergent STING-containing CBASS operons (Extended Data Figures 2a and 3a–c). Additionally, we determined 1.5 Å and 2.3 Å crystal structures for two CdnE homologues revealing an active enzyme conformation and unique substitutions in the nucleobase acceptor pocket consistent with adaptation for c-di-GMP synthesis (Extended Data Figures 2b and 3d–f)[15]. c-di-GMP is a common nucleotide second messenger used to regulate bacterial growth and intracellular signaling[18], and it is therefore difficult to conceive how bacteria could distinguish these functions of c-di-GMP from induction of CBASS immunity that results in rapid bacterial death[10,16,17]. To explain the

unexpected role of c-di-GMP in CBASS immunity, we analyzed the genomic context of all STING-containing CBASS operons and discovered that these systems are encoded almost exclusively in bacteria devoid of canonical GGDEF and EAL c-di-GMP signaling domains suggesting complete co-option of normal c-di-GMP function for a role in STING activation (Figure 2c).

Bacterial STINGs bind c-di-GMP with nanomolar affinity and exhibit a clear preference for canonical 3′–5′-linked cyclic dinucleotides (Figure 2d; Extended Data Figure 4a,b). In the *Fs*STING–3′,3′-cGAMP structure, the cyclic dinucleotide backbone is coordinated with N91 and N172, and each nucleobase is sandwiched between a stacking interaction formed with F92 and R153 (Figure 2e). In agreement with the strong preference of bacterial STING for c-di-GMP, a universally conserved D169 residue reads out the guanosine nucleobase by making a sequence-specific contact to the N2 position (Figure 2e). Using mutational analysis, we verified the importance of residues in the STING cyclic dinucleotide binding pocket and confirmed that conserved nucleobase contacts are required for c-di-GMP recognition (Extended Data Figures 5 and 6a–e). Human STING does not form prominent sequence-specific contacts with cyclic dinucleotides. Instead, human STING residue R232 makes additional contact to the phosphodiester backbone and is critical for high-affinity recognition of the mammalian cGAS product 2′–5′ / 3′–5′ cGAMP (2′,3′-cGAMP)[7,19]. A striking feature of bacterial STING receptors is an inability to recognize mammalian 2′,3′-cGAMP (Figure 2d; Extended Data Figure 4a,b). Cyclic dinucleotides occupy a similar compact conformation in both bacterial STING and human STING, but in bacterial STING the R232-equivalent position R151 is flipped outwards and does not contact the cyclic dinucleotide backbone (Extended Data Figure 1e). Additionally, a universally conserved T173 residue in bacterial STING located beneath the cyclic dinucleotide binding pocket reduces the space that would be necessary to accommodate a free 3′-OH within 2′,3′-cGAMP (Extended Data Figure 1f). We observed that bacterial STING is >1000× more sensitive to c-di-GMP than a synthetic analog with a 2′–5′ linkage (2′,3′-c-di-GMP) (Extended Data Figure 5g), further confirming the strict specificity of bacterial STING for 3′–5′-linked cyclic dinucleotides.

Activation of CBASS immunity induces bacterial growth arrest or cell death to destroy virally infected cells and limit phage propagation[10,16,17]. Bacterial STING domains occur primarily as fusions to a Toll/Interleukin-1 receptor (TIR) adaptor domain, or more rarely appended to predicted transmembrane segments (Figure 2a; Extended Data Figure 1a). TIR domains can function as NAD^+ (β-nicotinamide adenine dinucleotide) hydrolases in plant and animal immunity[20–22]. We therefore tested a full-length TIR-STING fusion from *Sphingobacterium faecium* (*Sf*STING; IMG Gene ID 2735805876) for catalytic function and observed rapid hydrolysis of NAD^+ to nicotinamide and adenine diphosphate-ribose (Figure 3a,b; Extended Data Figure 5a–d). *Sf*STING potently responds to c-di-GMP and weakly to 3′,3′-cGAMP, and catalysis is abolished by mutating a conserved TIR active-site glutamic acid (Figure 3b; Extended Data Figure 6f,g). Bacterial TIR-STING activation requires <100 nM c-di-GMP and results in cleavage of NAD^+ at 10× the rate observed for plant and animal TIR proteins involved in immune defense (Figure 3c; Extended Data Figure 5h,i). We expressed *Sf*STING in *E. coli* cells that synthesize c-di-GMP and observed potent growth inhibition (Figure 3d). *Sf*STING-induced toxicity is lost with a D259A

mutation that prevents c-di-GMP recognition and can be partially overcome with nicotinamide supplementation (Figure 3d; Extended Data Figure 6h,i), further supporting a role for bacterial STING in CBASS-mediated immunity as a c-di-GMP-responsive NADase effector.

Cyclic dinucleotide recognition drives bacterial STING oligomerization and formation of ordered filaments readily observable with negative stain electron microscopy (Figure 3e,f; Extended Data Figure 7). In the presence of activating c-di-GMP, *Sf*STING assembles into filaments typically 25–30 nm in length that exhibit four-fold symmetry and contain an ordered array of parallel-stacked homodimers (Figure 3f; Extended Data Figure 7j–l). Electron microscopy and biochemical analysis of *Sf*STING in the presence of the weak agonist 3′,3′-cGAMP reveals partial filament formation and STING complexes in a tetramer-like conformation, indicating that cyclic dinucleotide-stabilization of STING tetramers is likely required to seed filament growth (Figure 3e,f; Extended Data Figure 7j–l). Higher-order oligomerization is a known requirement for TIR activation[21,22], and mutations to the *Sf*STING cyclic dinucleotide binding domain that disrupt c-di-GMP-induced oligomerization prevent activation of TIR-STING NAD^+ cleavage (Extended Data Figure 6b,f,g). Remarkably, bacterial STING filament formation is consistent with a recently proposed model of human STING activation where parallel-stacking of STING homodimers initiates oligomerization and recruitment of the kinase TBK1[12,23]. Using the chicken STING cryo-electron microscopy structure as a guide[9], we constructed a model of bacterial STING oligomerization and identified surfaces in the bacterial STING domain at the beginning of helix α2 and end of helix α4 predicted to mediate oligomerization (Extended Data Figure 8a). Mutations to these surfaces do not disrupt *Sf*STING c-di-GMP-binding but prevent oligomerization into filaments (Extended Data Figure 8b,c). In the absence of filament formation all *Sf*STING NADase activity is lost (Extended Data Figure 8d) confirming that c-di-GMP-induced oligomerization is essential for TIR domain activation and effector function. These results define a core role of filament formation in STING activation and suggest that the primordial mechanism of STING signaling is cyclic dinucleotide-dependent effector oligomerization.

High-resolution crystal structures of *Fs*STING and *Cg*STING enabled construction of a structure-guided phylogenetic alignment of 103 bacterial and 492 metazoan STING proteins for comparative analysis of STING function and adaptation (Figure 4a; Extended Data Figures 9a and 10a). STING distribution is most consistent with a bacterial origin and acquisition into an early metazoan ancestor (Extended Data Figure 10a). The distinct cyclic dinucleotide binding pocket residues required for preferential recognition of c-di-GMP or 2′,3′-cGAMP are fixed and nearly exclusive to bacterial or metazoan STING sequences. Strict kingdom-specific conservation further supports 2′,3′-cGAMP as the dominant functional ligand throughout metazoan STING signaling, and suggests a clear transition occurred from c-di-GMP signaling in bacteria to noncanonical cyclic dinucleotide signaling in animals (Extended Data Figure 10b)[8,11,24]. We identified several instances of invertebrate metazoan TIR-STING fusions with a predicted architecture similar to bacterial STING, including within oyster genomes previously noted to encode dramatic expansions of innate immune receptors and predicted CD-NTase enzymes[8,24,25]. To further understand adaptation of STING to signaling in animal cells, we determined a 2.4 Å crystal structure of metazoan

TIR-STING from the Pacific oyster *C. gigas* (oyster TIR-STING). The full-length oyster TIR-STING structure reveals a domain-swapped configuration with a linker region that intertwines to connect the appended TIR effector module with the STING dimerization α-helix stem (Figure 4b). We next determined a 2.9 Å crystal structure of oyster TIR-STING in complex with 2′,3′-cGAMP confirming the phylogenetic analysis of strict retention of 2′,3′-cGAMP-interacting residues in invertebrate metazoan STING receptors (Figure 4b; Extended Data Figures 9f and 10b). Distinct from recent cryo-electron microscopy analysis of full-length human STING with the N-terminal transmembrane domain, no 180° rotation is observed in the linker connecting the oyster STING and TIR domains in the presence of 2′,3′-cGAMP[9]. Instead, closure of oyster STING around 2′,3′-cGAMP re-aligns inter-monomer contacts between the adjacent STING and TIR domains, inducing a downward 4° rotation in TIR domain orientation (Figure 4b). We did not observe oyster TIR-STING catalytic NAD^+ cleavage activity in the presence of cyclic dinucleotides, suggesting additional requirements for enzyme activation or that reorientation of the oyster STING TIR domain may instead facilitate protein–protein interactions similar to the signaling adaptor function of TIR domains in human MyD88 and TRIF (Extended Data Figure 9b–h)[26]. These results further explain adaptation of STING in metazoans and provide a molecular mechanism for how STING cyclic dinucleotide sensing is structurally communicated to appended effector modules.

Our data define a conserved mechanism of STING-dependent signaling shared in bacteria and human cells, and support a unified model to explain the emergence of cyclic dinucleotide sensing in animal innate immunity (Figure 4c)[8,11,24]. Bacterial STING proteins function as c-di-GMP receptors that control oligomerization-dependent activation of appended effector domains, and are frequently encoded in the genomes of *Bacteroidetes* species that grow as commensals enriched in human and animal microbiota[27]. Interestingly, c-di-GMP was the first discovered ligand of human STING[3], and human STING recognition of bacterial cyclic dinucleotides is critical for immune detection of intracellular pathogens such as *Listeria monocytogenes*[28–30]. Acquisition of STING as a c-di-GMP receptor could therefore provide an immediate selective advantage enabling animal cells to sense intracellular bacteria through detection of essential cyclic dinucleotide second messengers conserved in prokaryotes. Our structural analysis defines cyclic dinucleotide binding pocket mutations that adapted metazoan STING for recognition of endogenous 2′,3′-cGAMP signaling, and explains how emergence of metazoan-specific insertions enabled autophagy and type I interferon-dependent effector responses. Together with previous identification of diverse cGAS homologues and 2′–5′-linked signals in prokaryotic antiviral immunity[10,15,17], functional conservation of STING in bacteria reveals that each of the core protein components controlling human cGAS-STING signaling arose from an ancient mechanism of bacteriophage defense.

Methods

Phylogenetic distribution of STING-domain proteins in bacterial genomes

CBASS operons and STING proteins were taken from the list identified in[10,34] and supplemented by additional bacterial STING homologues identified using the “top IMG

homologue hits" function in the Integrated Microbial Genomes (IMG) database[35]. To assess the prevalence of c-di-GMP utilization in different phyla, Pfam annotation data of all genes in 38,167 bacterial and archaeal genomes were downloaded from the IMG database[35] in October 2017. Genomes were supplemented with 44 genomes manually identified with STING-containing operons that were absent from the October 2017 dataset. Genes annotated with the diguanylate cyclase GGDEF domain (pfam00990) or the diguanylate phosphodiesterase EAL domain (pfam00563) were counted for each phylum represented by at least 200 genomes in the database.

Protein expression and purification

Recombinant STING homologues were generated and purified as previously described[15,36]. Briefly, synthetic DNA constructs (Integrated DNA Technologies) were cloned via Gibson assembly into a modified pET16 vector for expression of recombinant N-terminal 6×His-, 6×His-SUMO2, or 6×His-MBP-SUMO2 fusion proteins in BL21-CodonPlus(DE3)-RIL *E. coli* (Agilent). Transformed bacteria were grown overnight in MDG media before inoculation in M9ZB media for large-scale protein expression (2–3× 1 L flasks, grown at 37°C with 230 rpm shaking). Once M9ZB cultures reached OD_{600} ~2.5, flasks were placed on ice for 20 min to slow bacterial growth. Cultures were induced with 500 μM final IPTG concentration and incubated at 16°C for ~20 h at 230 rpm. Cultures were harvested by centrifugation and the pellets were washed once with chilled PBS before flash freezing with liquid nitrogen and storage at −80°C. Functional bacterial TIR-STING constructs were expressed in cultures additionally supplemented with 10–30 mM nicotinamide to limit TIR toxicity.

Bacterial pellets were lysed by sonication in 1× lysis buffer (20 mM HEPES-KOH pH 7.5, 400 mM NaCl, 30 mM imidazole, 10% glycerol, and 1 mM DTT). Clarified lysates were purified by gravity-flow over Ni-NTA resin (Qiagen). Resin was washed with 1× lysis buffer supplemented to 1 M NaCl, and recombinant protein was eluted with 1× lysis buffer supplemented to 300 mM imidazole. Recombinant human SENP2 protease (D364–L589, M497A) was incubated with purified samples overnight during dialysis at 4°C against dialysis buffer (20 mM HEPES-KOH pH 7.5, 250 mM KCl, 10% glycerol, 1 mM DTT) to cleave the SUMO2 tag. Proteins were concentrated with 30 kDa-cutoff Amicon centrifuge filters (Millipore) before loading onto a 16/600 Superdex 200 size exclusion column equilibrated in gel filtration buffer (20 mM HEPES-KOH pH 7.5, 250 mM KCl, 1 mM TCEP). Protein purity was assessed by SDS-PAGE with Coomassie staining before concentrating samples to >10 mg ml^{-1}. Final proteins samples were flash frozen in liquid nitrogen and stored at −80°C.

Synthetic cyclic dinucleotide standards

Synthetic cyclic dinucleotide ligands used for structural biology and biochemistry experiments were purchased from Biolog Life Science Institute: 3′,3′-c-di-AMP (cat no. C 088), 3′,3′-c-di-GMP (cat no. C 057), 3′,3′-cGAMP (cat no. C 117), 2′,3′-cGAMP (cat no. C 161), 3′,3′-c-UMP–AMP (cat no. C 357), 2′,3′-c-di-GMP (cat no. C 182).

Protein crystallization and structure determination

Crystals for all proteins were initially grown at 18°C using the hanging drop vapor diffusion method. Concentrated protein stocks were thawed from −80°C on ice and diluted in buffer (25 mM HEPES-KOH pH 7.5, 70 mM KCl, 1 mM TCEP) to final concentration. STING–cyclic dinucleotide complexes were formed by incubating protein with ligand on ice for 20 min before setting trays. In all cases, optimized crystals were obtained using EasyXtal 15-Well hanging drop trays (Qiagen) in 2 μl drops mixed 1:1 over a 350 μl reservoir of mother liquor after 1–3 days of growth at 18°C. Final optimized crystal growth conditions were as follows: Crystals of native and selenomethionine-substituted *Fs*STING bound to 3′,3′-cGAMP grew at 10 mg ml^{-1} with 0.5 mM 3′,3′-cGAMP in 2 M ammonium sulfate, 0.2 M sodium acetate pH 4.5 and were cryoprotected with NVH oil (Hampton). Crystals of selenomethionine-substituted *Cg*STING grew at 18 mg ml^{-1} with 0.5 mM c-di-GMP in 0.1 M HEPES-NaOH pH 7.5, 20% PEG-10,000 and were cryoprotected with mother liquor supplemented with 20% ethylene glycol (*Cg*STING continually precipitated upon incubation with c-di-GMP likely resulting in specific crystallization of the soluble apo form. Crystals of selenomethionine-substituted *Fs*CdnE grew at 7 mg ml^{-1} with 10.5 mM $MgCl_2$ and 0.5 mM GpCpp in 0.1 M sodium acetate pH 4.6, 2 M sodium formate and were cryoprotected by supplementing reservoir solution with 25% ethylene glycol and 0.5 mM GpCpp. Crystals of selenomethionine-incorporated *Cg*CdnE grew at 7 mg ml^{-1} with 10.5 mM $MgCl_2$ and 0.5 mM GpCpp and grew in 0.2 M sodium thiocyanate, 20% PEG-3350 and were cryoprotected with NVH oil (Hampton). No GpCpp density is visible in either of the *Fs*CdnE or *Cg*CdnE crystal structures. Crystals of apo oyster TIR-STING (*Crassostrea gigas* XP_011430837.1) grew at 7 mg ml^{-1} in 0.2 M $MgCl_2$, 0.1 M Tris pH 8.5, and 16% PEG-4000 and were cryoprotected by supplementing mother liquor with 20% glycerol. Crystals of oyster TIR-STING bound to 2′,3′-cGAMP grew at 7 mg ml^{-1} protein with 0.5 mM 2′,3′-cGAMP in 0.2 M ammonium citrate pH 7.0, 20% PEG-3350 and were cryoprotected with mother liquor supplemented with 20% ethylene glycol and 0.5 mM 2′,3′-cGAMP. X-ray diffraction data were collected with single crystals at the Advanced Photon Source (beamlines 24-ID-C and 24-ID-E) with a wavelength of 0.97918 Å and temperature of 80°K.

Data were processed with XDS and AIMLESS[37] using the SSRL autoxds script (A. Gonzalez, Stanford SSRL). Experimental phase information for all proteins was determined using data collected from selenomethionine-substituted crystals. Anomalous sites were identified and an initial map generated with AutoSol within PHENIX 1.17 (ref 38). Iterative model building and refinement was performed using Coot 0.8.9 (ref 39) and PHENIX. Final structures were refined to stereochemistry statistics for Ramachandran plot (favored / allowed), rotamer outliers, and MolProbity score as follows: *Fs*STING–3′,3′-cGAMP, 97.49% / 2.51%, 1.12%, and 1.26; *Cg*STING apo, 97.23% / 2.77%, 1.90%, and 1.55; *C. gigas* STING apo, 95.68% / 4.32%, 0.72%, and 1.58; *C. gigas* STING–2′,3′-cGAMP, 97.25% / 2.75%, 0.67%, and 1.38; *Fs*CdnE apo, 98.86% / 1.14%, 0.30%, and 0.97; *Cg*CdnE, 98.63% / 1.37%, 0.70%, and 1.09. See Supplementary Table 1 and ‘Data availability’ for deposited PDB codes. All structure figures were generated with PyMOL 2.3.4.

Structure-guided alignment of bacterial and metazoan STING domains

To guide alignment and phylogenetic analysis of all STING family receptors, the bacterial *Fs*STING, *Cg*STING, and oyster STING structures were superposed with human STING and representatives from all previously published metazoan STING structures[6–9,12,19,23,40–46] using the secondary-structure matching algorithm in Coot[39,47]. A sequence alignment was extracted from the superposed structures according to C-alpha position, and extended to include a list of all known STING protein sequences using PROMALS3D[48]. Briefly, the list of bacterial STING protein sequences was prepared from analysis of bacterial defense islands as described above and included 103 sequences. Sequences were aligned with MAFFT[49] and manually trimmed in Jalview[50] based on boundaries of the *Fs*STING crystal structure to remove effector domain sequences and obtain an alignment of the STING cyclic dinucleotide binding domain. Metazoan STING sequences were obtained from the Interpro (IPR033952) and PFam (PF15009) databases and trimmed to the cyclic dinucleotide binding domain based on boundaries of the human STING and oyster STING crystal structures resulting in 492 unique sequences. The output PROMALS3D alignment was inspected to ensure accurate secondary structure matching between bacterial and metazoan STING and includes 34 gap-free sites. A STING family phylogenetic tree was then calculated using the MAFFT server and visualized with iTOL[51] for analysis.

Cyclic dinucleotide synthesis and thin-layer chromatography analysis

CdnE homologues were tested for cyclic dinucleotide synthesis capability using α^{32}P-labeled NTPs and product resolution with thin-layer chromatography as previously described[15]. In a 20 μl final reaction volume, 5 μM enzyme was incubated with 25 μM of each cold NTP (ATP, GTP, CTP, UTP; 100 μM total) and with trace radiolabeled NTP (~1 μCi) as indicated for 3 h at 37°C in buffer containing 50 mM Tris-HCl pH 7.5, 50 mM KCl, 10 mM $Mg(OAc)_2$, and 1 mM TCEP. Reactions were treated with Calf Intestinal Phosphatase (New England Biolabs) at 37°C for 30 min to remove excess starting nucleotides. 0.5 μl of sample was separated on a PEI-Cellulose F TLC plate (EMD Biosciences) using a running solvent of 1.5 M KH_2PO_4 pH 3.8 for 0.5–1 h. Plates were dried for 1 h at ambient temperature before exposure to a phosphor-screen and imaging with a Typhoon Trio Variable Mode Imager (GE Healthcare). Control cyclic dinucleotides were generated with recombinant purified *Mus musculus* cGAS, *Vibrio cholerae* DncV, *Bacillus thuringiensis* DisA, *Escherichia coli* CdnE, and *Pseudomonas aeruginosa* WspR (with D70E constitutively activating mutation) as previously described[15,52]. cGAS reactions were additionally supplemented with 5 μM ISD45 dsDNA for enzyme activation[36]. *E. coli* CdnE reactions to generate 3′,3′-c-UMP–AMP were conducted at pH 9.4 with 50 mM CAPSO.

STING-cyclic dinucleotide complex formation and electrophoretic mobility shift assay

STING interactions with cyclic dinucleotide ligands were monitored by electrophoretic mobility shift assay as previously described[8]. 10 μl reactions were generated in reaction buffer (5 mM $Mg(OAc)_2$, 50 mM Tris-HCl pH 7.5, 50 mM KCl, and 1 mM TCEP) with 20 μM final protein concentration and ~1 μM α^{32}P-labeled cyclic dinucleotides (~0.1 μCi). Protein titration reactions utilized serial dilutions of stock protein to final concentrations

ranging from 0.3 nM to 150 μM with ~250 nM cyclic dinucleotide. Reactions were incubated at 25°C for 5 min prior to resolution on a 7.2 cm 6% nondenaturing polyacrylamide gel run at 100 V for 45 min in 0.5× TBE buffer. The gel was fixed for 15 min in a solution of 40% ethanol and 10% acetic acid before drying at 80°C for 1 h. The dried gel was exposed to a phosphor-screen and imaged on a Typhoon Trio Variable Mode Imager (GE Healthcare). Signal intensity was quantified using ImageQuant 5.2 software.

TIR NAD^+ cleavage activity analysis with fluorescent ε-NAD

Plate reader reactions were prepared in a 96-well plate format in 50 μl final volume with reaction buffer (20 mM HEPES-KOH pH 7.5, 100 mM KCl), 500 μM ε-NAD, 500 nM protein, and between 1 nM – 100 μM cyclic dinucleotide as indicated. Briefly, a master-mix was prepared on ice containing each ligand and protein was added immediately before beginning analysis. 96-well plates were read continuously over 1 h using a Synergy H1 Hybrid Multi-Mode Reader (BioTek) in fluorescence mode at 410 nm after excitation at 300 nm. Reactions were performed in technical duplicate and data are representative of independent biological replicates. Error bars indicate standard error of the mean for biological replicates. TIR oligomerization dependence experiments were performed in the absence of cyclic dinucleotide using glutathione or nickel-NTA resin at a 1:1 ratio as previously described[21,22]. Resin was pre-equilibrated and re-suspended in 100 μl of buffer containing 500 nM protein, 20 mM HEPES-KOH pH 7.5, 100 mM KCl, and 500 μM ε-NAD, and 50 μl of mixture was used for analysis.

HPLC TIR NAD^+ cleavage activity analysis

High-pressure liquid chromatography was used to measure TIR-STING NAD^+ cleavage activity and to directly observe product formation. Reactions were prepared in 20 mM HEPES-KOH pH 7.5, 100 mM KCl at a final concentration of 500 nM enzyme with or without addition of 10 μM of cyclic dinucleotides or as indicated. TIR-STING and cyclic dinucleotide ligands were incubated on ice for 10 min prior to addition of NAD^+ at 500 μM. Reactions were incubated for 1 h at 25°C, and then heat-inactivated at 95°C for 1 min and incubation on ice for at least 5 min. Reactions were filtered through Millipore Amicon Ultra-0.5 ml filters with a 30 kDa cutoff by centrifugation for 10 min at 9,300 × g to remove protein before HPLC analysis. Products were separated and analyzed by HPLC with absorbance monitoring at 254 nm. Samples were injected onto a C18 column (Zorbax Bonus-RP 4.6×150 mm, 3.5-μm) attached to an Agilent 1200 Infinity Series LC system. Two separate elution strategies were utilized: 1) Isocratic elution at 40°C with a flow rate of 1 ml min^{-1} with 50 mM NaH_2PO_4 pH 6.8 supplemented with 3% acetonitrile. 2) Gradient elution at 50°C with a flow rate of 1 ml min^{-1} using solvent A (10 mM NH_4OAc) and solvent B (100% methanol), and a gradient from 5–100% solvent B over 12 min.

Reactions to measure discontinuous kinetics were assembled on ice in reaction buffer (20 mM HEPES-KOH pH 7.5, 100 mM KCl) with final concentration of 50 nM protein, 2 μM c-di-GMP, and indicated concentrations of NAD^+. Reactions were started simultaneously and quenched after 10, 30, 120, 300, and 600 s. Products were analyzed by HPLC as described above, product ADPr peaks were integrated for each time point, and concentrations were calculated according to a standard curve. Data were analyzed using GraphPad Prism 8.4.2

software and the kinetics data fitted using a Michaelis-Menten model to calculate K_M and V_{max}. Results are representative of two independent biological replicates and plotted with errors bars denoting the standard deviation.

STING toxicity analysis in *E. coli*

*Sf*STING and mutant constructs were cloned into pBAD33 for arabinose-inducible expression in *E. coli* strain MG1655. Cells were transformed by electroporation, four colonies for each construct were sequence verified and used to inoculate individual LB liquid cultures supplemented with 30 μg ml^{-1} chloramphenicol for 6 h at 37°C with 200 rpm shaking. Cultures were diluted 1:10 into fresh LB medium with 30 μg ml^{-1} chloramphenicol, and 180 μl of diluted cultures were divided into wells in a 96-well plate. Plate cultures were supplemented with 0.2% arabinose and 30 mM nicotinamide as indicated to a final volume of 200 μl per well. OD_{600} was followed using a TECAN Infinite 200 plate reader with measurement every 10 min.

Electron microscopy sample preparation, data collection, and processing

Samples for negative-stain electron microscopy analysis were prepared by diluting purified *Sf*STING (E84A mutation) protein alone, or with an equimolar ratio cyclic dinucleotide as indicated, to a concentration of 50 μM in gel filtration buffer (20 mM HEPES-KOH pH 7.5, 150 mM KCl, 1 mM TCEP). Protein samples were further serially diluted in gel filtration buffer to a final concentration of 0.026 mg ml^{-1}. For protein–ligand mixtures, gel filtration buffer was supplemented with 1 μM of ligand for each serial dilution step. 3 μl of the diluted sample was applied onto a glow-discharged (30 s, 30 mA) 400-mesh copper grid (Electron Microscopy Sciences) coated with an ~10 nm layer of continuous carbon (Safematic CCU-010), followed by a 30 s absorption step and side blotting to remove bulk solution. The grid was immediately stained with 1.5% uranyl formate and then blotted from the side. The staining procedure was repeated twice with a 30 s incubation with uranyl formate before the final blotting step. The grid was air dried prior to imaging.

Electron microscopy Images for 2D classification were collected using an FEI Tecnai T12 transmission electron microscope operating at 120 keV and equipped with a Gatan 4K × 4K CCD camera at a nominal magnification of 67,000×, pixel size of 1.68 Å, at a nominal defocus range of 1.0–2.0 μm. Electron microscopy images for *Sf*STING oligomerization mutants (R307E, A309R; L201R, D203R; Δ L275–Q282) were collected using a Philips CM10 transmission electron microscope operating at 100 keV and equipped with a Gatan UltraScan 894 (2k × 2k) CCD camera at a nominal magnification of 52,000×, pixel size of 2.06 Å, at a nominal defocus range of 1.5 μm.

Micrographs were converted to JPEG format using e2proc2d.py script[53]. All image processing was performed in RELION-3[54]. After CTF estimation with GCTF[55], particle picking was carried out with gautomatch (Kai Zhang, https://www.mrc-lmb.cam.ac.uk/kzhang/) followed by manual review. Where present, fibers were picked separately and treated as independent datasets. Particles were extracted with a 224 pixel box size (~375 Å) and subjected to one round of 2D reference-free classification to generate 2D class averages.

Size-exclusion chromatography with multi-angle light scattering

Purified protein samples for SEC-MALS analysis were diluted in ice-cold running buffer (150 mM KCl, 20 mM HEPES-KOH pH 7.5, and 1 mM TCEP) to a final concentration of 2 mg ml^{-1}. Samples including ligand were prepared with 100 μM cyclic dinucleotide and incubated on ice for at least 5 min. All samples were subjected to brief centrifugation (21,000 × g, 5 min, 4°C) to remove precipitated protein before injection onto an SRT SEC-300 column (SEPAX). Refractive index (dRI) was measured with a Wyatt Optilab T-rex Refractive Index Detector and protein concentration estimated assuming a dn/dc of 0.185. The system was also equipped with a Wyatt Dawn Heleos II Multi-Angle Light Scattering detector used to determine molar mass. All analysis was carried out using ASTRA 7 software and figures produced with GraphPad Prism 8.4.2.

Reporting summary

Further information on research design is available in the Nature Research Reporting Summary linked to this paper.

Data Availability Statement

Data that support the findings of this study are available within the article and its Extended Data and Supplementary Tables. Integrated Microbial Genomes (IMG) database accessions are listed in Extended Data Figure 1 and Protein Data Bank (PDB) database accessions are listed in each figure legend. Coordinates and structure factors of *Fs*STING–3′,3′-cGAMP, *Cg*STING, oyster TIR-STING, oyster TIR-STING–2′,3′-cGAMP, *Fs*CdnE, and *Cg*CdnE have been deposited in PDB under accession codes 6WT4, 6WT5, 6WT6, 6WT7, 6WT8, and 6WT9.

Extended Data

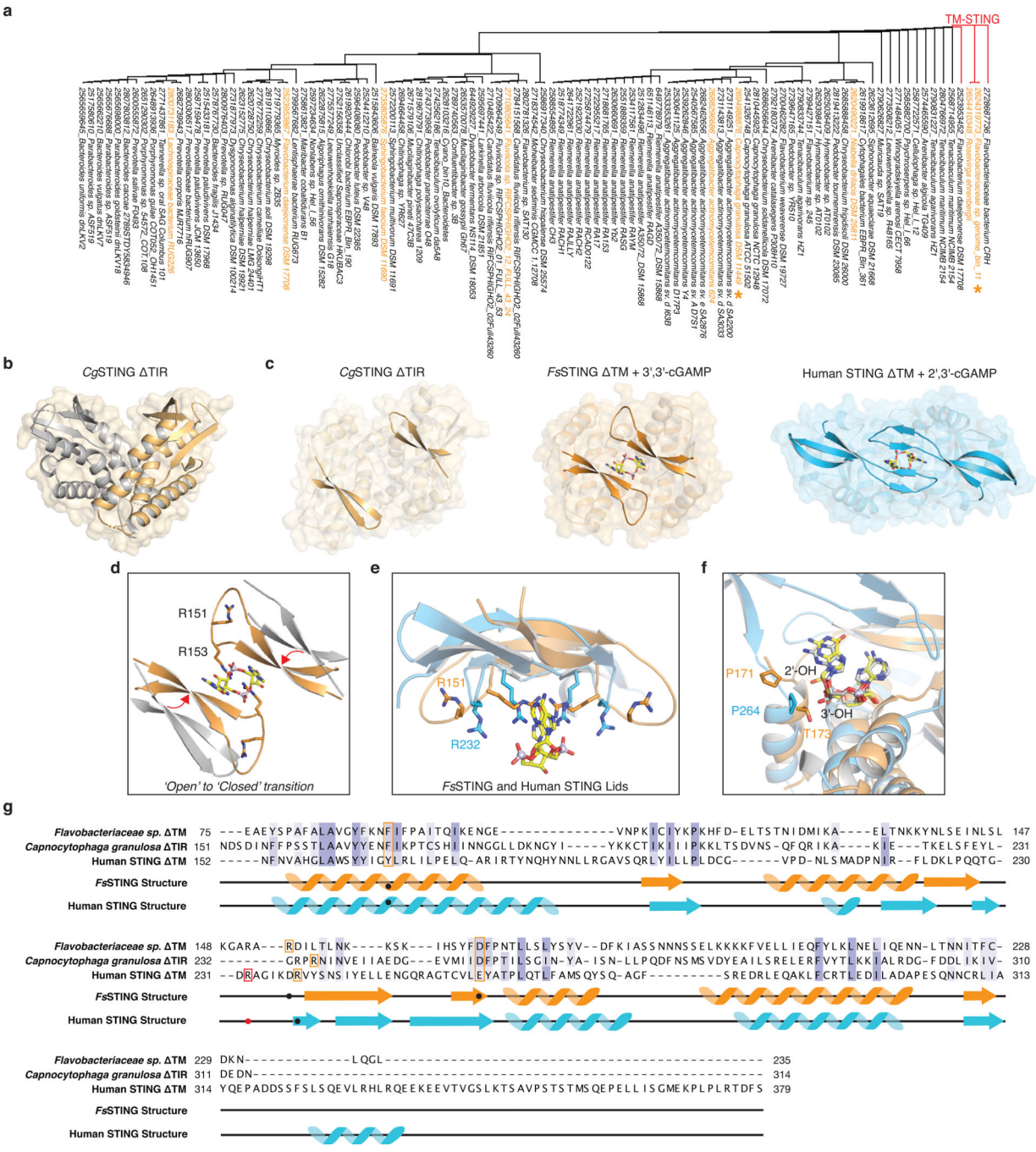

Extended Data Figure 1 |. Structural analysis of bacterial STING–cyclic dinucleotide complex formation.

a, Phylogenetic tree of all CBASS-associated bacterial STING homologues based on structure-guided sequence alignment and previous bioinformatic analysis[10,34]. STING homologues investigated in this study are highlighted in orange, and a star denotes determined STING crystal structures. All TM-STING fusions cluster together.

b, Crystal structure of a STING receptor from the bacterium *Capnocytophaga granulosa* (*Cg*STING) in the apo state reveals an open configuration with a solvent exposed cyclic dinucleotide-binding pocket at the dimeric interface (monomers in gold and grey for clarity). The *Cg*STING structure confirms that both divergent TM-STING and TIR-STING fusions are members of the same structurally conserved family of STING receptors.
c, Comparison of the *Cg*STING, *Fs*STING–3′,3′-cGAMP, and human STING–2′,3′-cGAMP structures demonstrates conservation of an open-to-closed β-strand lid movement upon ligand binding.
d, Overlay of the β-strand lid of *Cg*STING (grey) and *Fs*STING (orange) shows both inward translation and slight rotation resulting in a displacement of ~5 Å. R153 of *Fs*STING stacks between the bases of 3′,3′-cGAMP while R151 is splayed away from ligand.
e, Comparison of the human STING and *Fs*STING lid region shows conserved contacts from β-strand arginine residues. Unlike in bacterial STING, human STING R232 makes an additional contact with the cyclic dinucleotide phosphodiester backbone that is critical for recognition of the 2′–5′ linkage in 2′,3′-cGAMP. See also Extended Data Figure 10b for detailed comparison.
f, Modeling of 2′,3′-cGAMP into the *Fs*STING–3′,3′-cGAMP structure demonstrates an additional feature of bacterial STING preventing recognition of 2′–5′-linked cyclic dinucleotides. Although the overall cyclic dinucleotide conformation is shared between human and bacterial STING, the α-helix ending at P264 in human STING is a half turn longer in *Fs*STING (also ending in a proline) which places a conserved T173 residue in a position that occludes where the free 3′-OH of 2′,3′-cGAMP would be positioned.
g, Structure-guided alignment of *Fs*STING and human STING cyclic dinucleotide binding domains. *Fs*STING and human STING exhibit no detectable sequence homology but share a conserved structural fold. Key residues involved in cyclic dinucleotide binding that are shared between bacterial and human STING are boxed in orange and human STING specific cyclic dinucleotide contacts are boxed in red. In *Fs*STING, D169 directly reads out the guanine base of c-di-GMP.

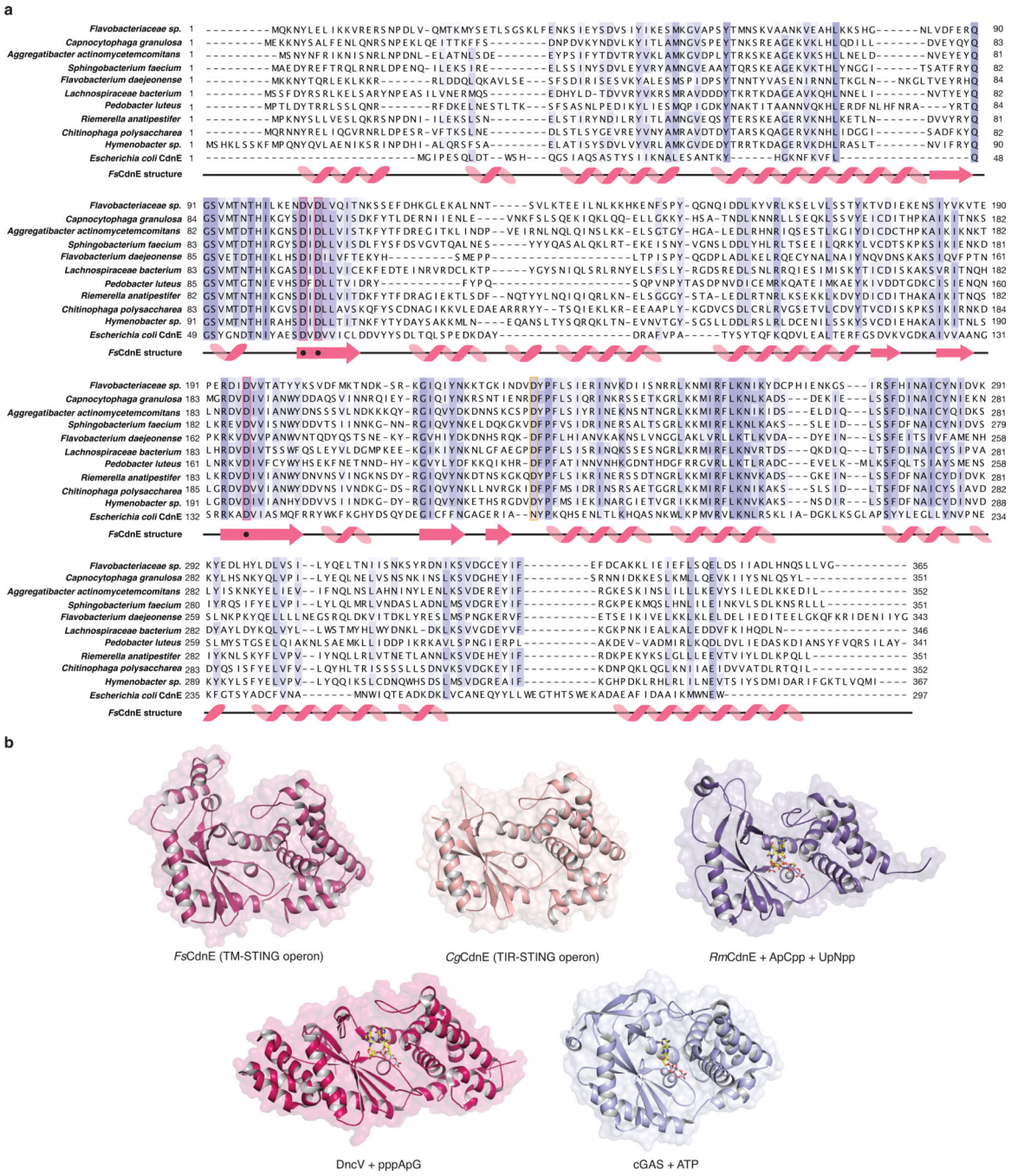

Extended Data Figure 2 |. Structural analysis of STING-associated CD-NTase enzymes.

a, Sequence and secondary structure alignment of STING-associated CD-NTases reveals the extent of homology between CdnE homologues from unrelated bacterial strains. Highlighted positions include active-site residues (pink box), and an aspartic acid substitution at a position known to be involved in nucleotide substrate selection (orange box) that is unique to CD-NTases in STING-containing CBASS operons[15]. A divergent *E. coli* CdnE that synthesizes cyclic UMP–AMP is included for comparison.

b, Crystal structures of *Fs*CdnE and *Cg*CdnE from STING-containing CBASS operons allow direct comparison with previously determined bacterial and human CD-NTase structures. The *Fs*CdnE and *Cg*CdnE structures are most closely related to the Clade E CD-NTase structure from *Rhodothermus marinus* CdnE (*Rm*CdnE). *Rm*CdnE PDB 6E0L[15], *V. cholerae* DncV PDB 4TY0[56], human cGAS PDB 6CTA (DNA omitted for clarity)[36].

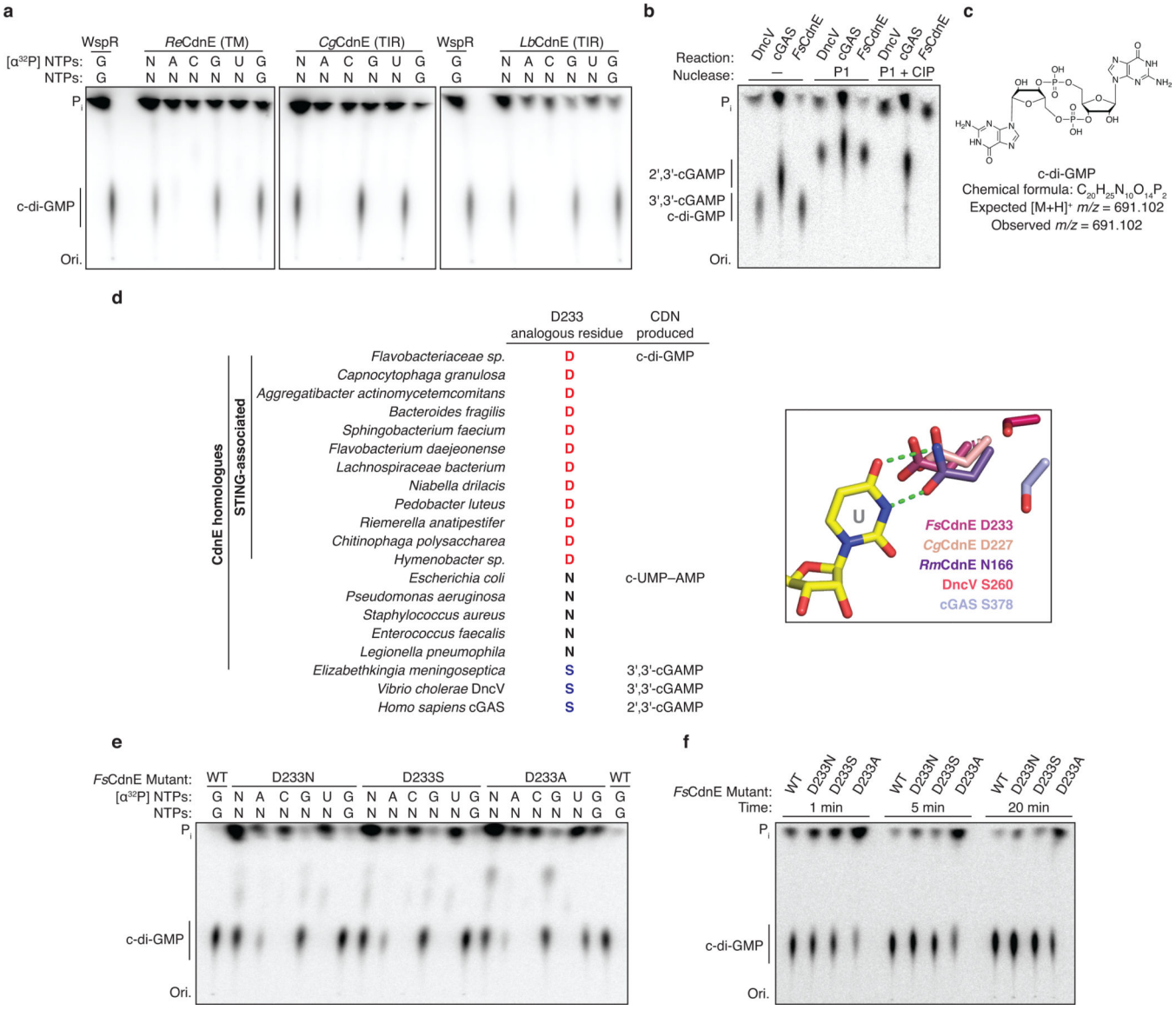

Extended Data Figure 3 |. Biochemical analysis of c-di-GMP synthesis by bacterial STING-associated CD-NTases.

a, In addition to *Fs*CdnE (see Figure 2b), CdnE homologues from three divergent STING-containing CBASS operons were purified and tested for cyclic dinucleotide synthesis specificity using α^{32}P-radiolabeled NTPs and thin-layer chromatography. Deconvolution experiments show a single major product requiring only GTP which migrates identically to c-di-GMP synthesized by the GGDEF enzyme WspR. All reactions were treated with alkaline phosphatase to remove exposed phosphates. Of note, only two bacterial genomes

encoding a STING-containing CBASS operon retain proteins with a predicted canonical GGDEF c-di-GMP signaling domain. The exceptions are *Chlorobi bacterium EBPR_Bin_190* which contains a single GGDEF domain that is fused to a SLATT domain and may be part of a CBASS-like system[10] and a *Lachnospiraceae bacterium RUG226* genome that encodes many GGDEF genes. The *Lachnospiraceae bacterium RUG226* CdnE retains exclusive production of c-di-GMP suggesting the CdnE-STING system is sequestered in this bacterium or that an unknown mechanism may exist to prevent toxic STING activation. *Re*CdnE, *Roseivirga ehrenbergii*; *Cg*CdnE, *Capnocytophaga granulosa*; *Lb*CdnE, *Lachnospiraceae bacterium*; N, all four rNTPs; P_i, inorganic phosphate; Ori., origin. Data are representative of 2 independent experiments.

b, Nuclease treatment confirms that the *Fs*CdnE enzymatic product contains only canonical 3′–5′ phosphodiester bonds. The α^{32}P-GTP cyclic dinucleotide product is susceptible to cleavage by nuclease P1 resulting in release of GMP as a new species which migrates further up the TLC plate. Further digestion with calf-intestinal phosphatase (CIP) removes all exposed phosphates resulting in complete loss of a labeled product spot. DncV (Dinucleotide cyclase in *Vibrio*) derived 3′,3′-cGAMP is similarly susceptible to complete digestion by P1 and CIP treatment whereas 2′,3′-cGAMP synthesized by mouse cGAS in only partially digested due to the presence of the non-canonical 2′–5′ bond. Data are representative of 2 independent experiments.

c, High-resolution mass spectrometry analysis confirms the identity of the major *Fs*CdnE enzymatic product as canonical c-di-GMP. Chemically synthesized c-di-GMP was used for direct spectral comparison.

d, Sequence alignment and zoom-in inset of the active-site of the *Rm*CdnE structure in complex with nonhydrolyzable UTP and ATP analogs (PDB 6E0L) demonstrating a contact in the CD-NTase lid domain known to control nucleobase sequence specificity[15]. *Rm*CdnE synthesizes cyclic UMP–AMP and uses N166 to specifically contact the uridine Watson-Crick edge. In contrast, *Fs*CdnE and *Cg*CdnE contain an aspartic acid substitution at this position and synthesize c-di-GMP, and *Vibrio cholerae* DncV and human cGAS contain a serine substitution at this position and synthesize 3′,3′-cGAMP and 2′,3′-cGAMP. 93% of STING-associated CD-NTase enzymes (96 of 103) contain a conserved aspartic acid at the *Fs*CdnE D233 position consistent with strict specificity of c-di-GMP as the nucleotide second messenger controlling bacterial STING activation. *Rm*CdnE PDB 6E0L[15], *V. cholerae* DncV PDB 4TY0[56], human cGAS PDB 6CTA (DNA omitted for clarity)[36].

e,**f**, Mutational analysis of the importance of D233 in *Fs*CdnE c-di-GMP synthesis activity. D233 substitutions do not disrupt the overall ability of *Fs*CdnE to selectively synthesis c-di-GMP, but a D233A substitution causes a mild reduction in nucleobase selectivity and efficiency of c-di-GMP synthesis. These results are consistent with a role for D233 in nucleobase selection but demonstrate full selectively is achieved by additional contacts in the active site pocket. Data are representative of 3 independent experiments.

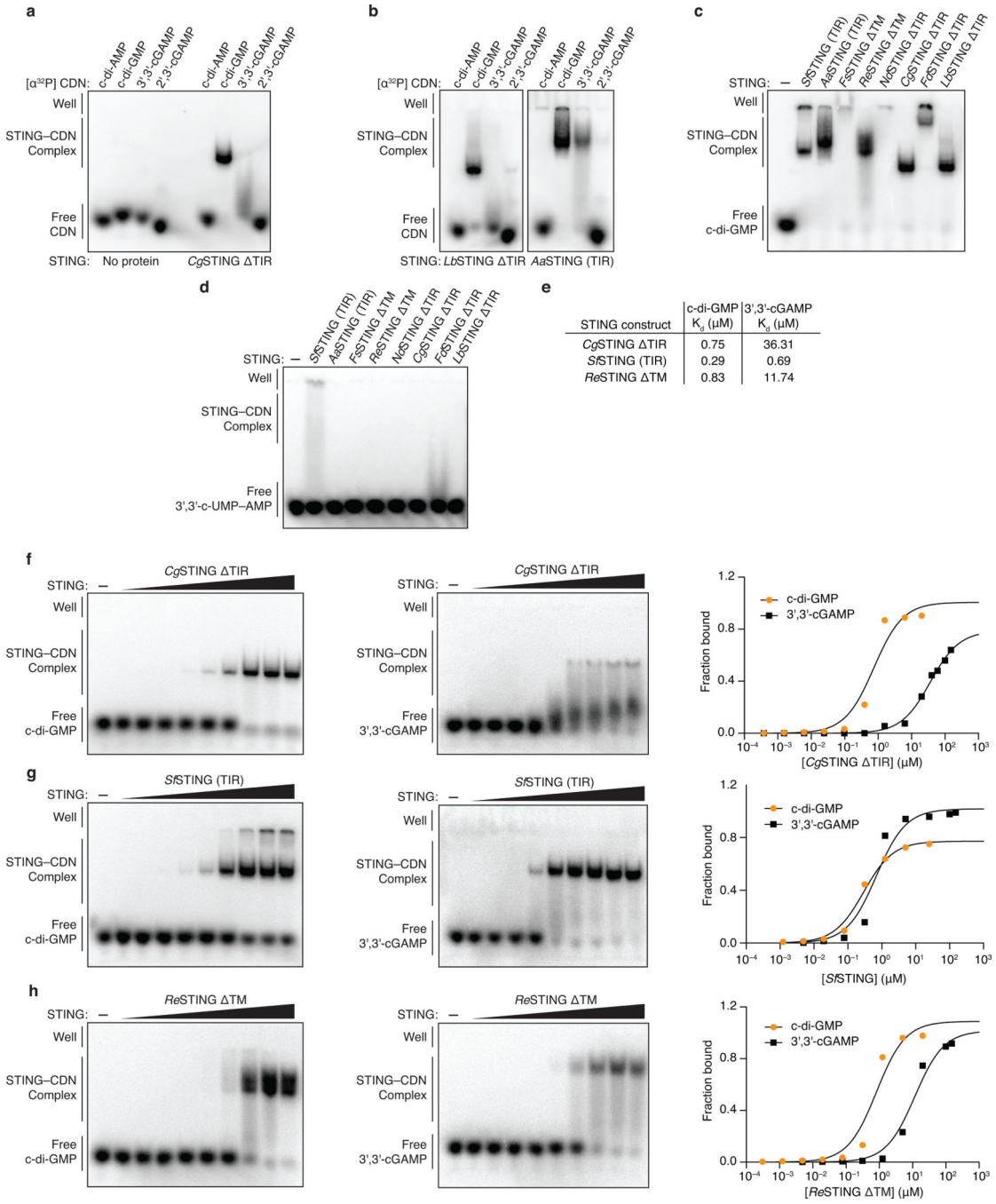

Extended Data Figure 4 |. Biochemical analysis of bacterial STING cyclic dinucleotide recognition specificity.

a,**b**, Electrophoretic mobility shift assay (EMSA) of purified bacterial STING proteins with radiolabeled cyclic dinucleotide (CDN) ligands. Bacterial STING receptors specifically recognize c-di-GMP and have a weak ability to bind 3′,3′-cGAMP. No interaction was observed with c-di-AMP or 2′,3′-cGAMP. *Capnocytophaga granulosa* (CgSTING), *Lahnospiraceae bacterium* STING (*Lb*STING), *Aggregatibacter actinomyetemcomitans* STING (*Aa*STING). Data are representative of 2 independent experiments.

c, EMSA analysis of a diverse panel of bacterial STING homologues demonstrates conservation of c-di-GMP binding in both TM-STING and TIR-STING CBASS immunity. *Nd*STING (*Niabella drilacis*) and *Fd*STING (*Flavobacterium daejeonense*). Higher-order complex formation visible as well-shifted complexes is consistent with STING oligomerization results (see Figure 3f and Extended Data Figure 7). Data are representative of 3 independent experiments.

d, EMSA analysis of diverse bacterial STING homologues broadly demonstrates no interaction with the 3′,3′-c-UMP–AMP second messenger synthesized by the divergent CD-NTase *E. coli* CdnE[15] and further confirms the specificity of c-di-GMP signaling in bacterial STING-containing CBASS operons. Data are representative of 2 independent experiments.

e,**f**,**g**,**h**, EMSA analysis and quantification of the affinity of bacterial STING homologues for c-di-GMP and 3′,3′-cGAMP. Signal intensity analysis is plotted as fraction bound (shifted / total signal) as a function of increasing protein concentration and fit to a single binding isotherm. *Cg*STING and *Re*STING have a >10-fold preference for c-di-GMP while *Sf*STING has a similar apparent affinity for c-di-GMP and 3′,3′-cGAMP. Data are representative of 2 independent experiments.

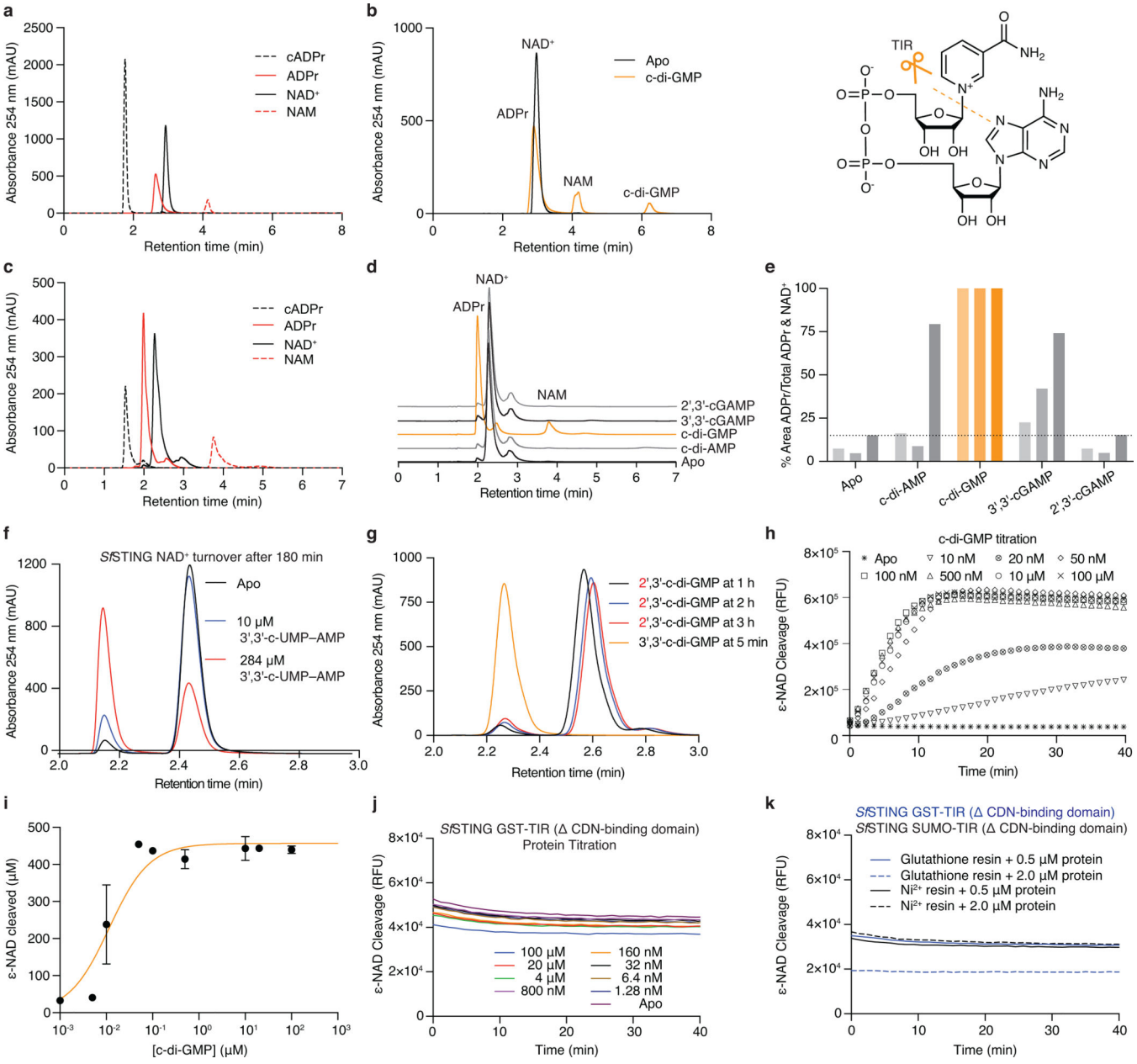

Extended Data Figure 5 |. Bacterial STING activation of TIR NADase activity.

a, HPLC analysis of chemical standards separated with an ammonium acetate:methanol gradient elution used to analyze bacterial TIR-STING activity (see Methods). The NAD^+ and ADPr peaks have overlapping bases under these conditions. cADPr, cyclic adenosine diphosphate-ribose; ADPr, adenosine diphosphate-ribose; NAD^+, β-nicotinamide adenine dinucleotide; NAM, nicotinamide.

b, HPLC analysis of *Sf*STING NAD^+ cleavage activity with gradient elution. *Sf*STING at 500 nM protein with 2 μM c-di-GMP converts 500 μM NAD^+ into ADPr and NAM in 30 min at ambient temperature. *Sf*STING does not generate any cyclized product and is therefore a standard glycosyl hydrolase. Inset: Schematic of NAD^+ cleavage reaction.

c, HPLC analysis of chemical standards separated with an alternative isocratic elution strategy (see Methods) that results in clearer separation of NAD^+ and ADPr peaks.
d, HPLC analysis of *Sf*STING NAD^+ cleavage activity with isocratic elution. *Sf*STING NAD^+ cleavage activity requires specific activation with c-di-GMP (30 min reactions).
e, HPLC analysis of *Sf*STING NAD^+ cleavage activity and cyclic dinucleotide agonist specificity. Each reaction was tested with 500 nM *Sf*STING, 500 μM cyclic dinucleotide, and 500 μM NAD^+ and sampled at 45, 90 or 180 min (gradient coloring in bars). *Sf*STING preferentially responds to c-di-GMP, but 3′,3′-cGAMP and c-di-AMP can function as weak agonists. Data are representative of 3 independent experiments.
f, HPLC analysis of *Sf*STING NAD^+ cleavage activity in the presence of 3′,3′-c-UMP–AMP. 3′,3′-c-UMP–AMP is a >1000× weaker agonist than c-di-GMP. Data are representative of 3 independent experiments.
g, HPLC analysis of *Sf*STING NAD^+ cleavage activity in the presence of a synthetic c-di-GMP analog with a noncanonical 2′–5′ linkage (2′,3′-c-di-GMP). 2′,3′-c-di-GMP is not capable of stimulating robust *Sf*STING activation even at very high concentrations (250 μM vs. 250 nM canonical c-di-GMP), confirming the specificity of bacterial STING for 3′–5′-linked cyclic dinucleotides. Data are representative of 3 independent experiments.
h, Plate reader analysis of *Sf*STING NAD^+ cleavage activity using the fluorescent substrate ε-NAD. ε-NAD increases in fluorescence intensity after cleavage. *Sf*STING exhibits rapid catalysis with complete turnover at 500 nM protein with 500 nM c-di-GMP after 10 min at 25°C. No background activity is observed in the absence of ligand. Data are representative of 3 independent experiments.
i, Plate reader analysis of *Sf*STING NAD^+ cleavage activity in the presence of 500 nM protein with increasing c-di-GMP concentration reveals that low nM c-di-GMP levels are sufficient to induce ε-NAD cleavage. Greater c-di-GMP concentrations are required for maximal activity consistent with binding data and the higher amount of c-di-GMP required for complete stabilization of the *Sf*STING–c-di-GMP complex (See Extended Data Figure 4e–h). Saturation occurs above 100 nM c-di-GMP with 40 min reactions. Data are ± s.d. of n = 3 technical replicates and are representative of 3 independent experiments.
j,**k**, TIR-domain NAD^+ cleavage activity requires protein oligomerization. For other systems[21,22], TIR activation has been observed at very high *in vitro* protein concentrations or in the presence of affinity resins as an artificial oligomerization-inducing matrix[21,22]. We used a GST-TIR construct to express the *Sf*STING TIR domain in absence of the STING cyclic dinucleotide binding domain and observed that even at >200× the concentrations for which the full-length protein shows c-di-GMP induced activity, or in the presence of multivalent affinity resin, no NAD^+ cleavage activity occurs. These results demonstrate NAD^+ cleavage activity specifically requires STING cyclic dinucleotide recognition for activation. Data are representative of 2 independent experiments.

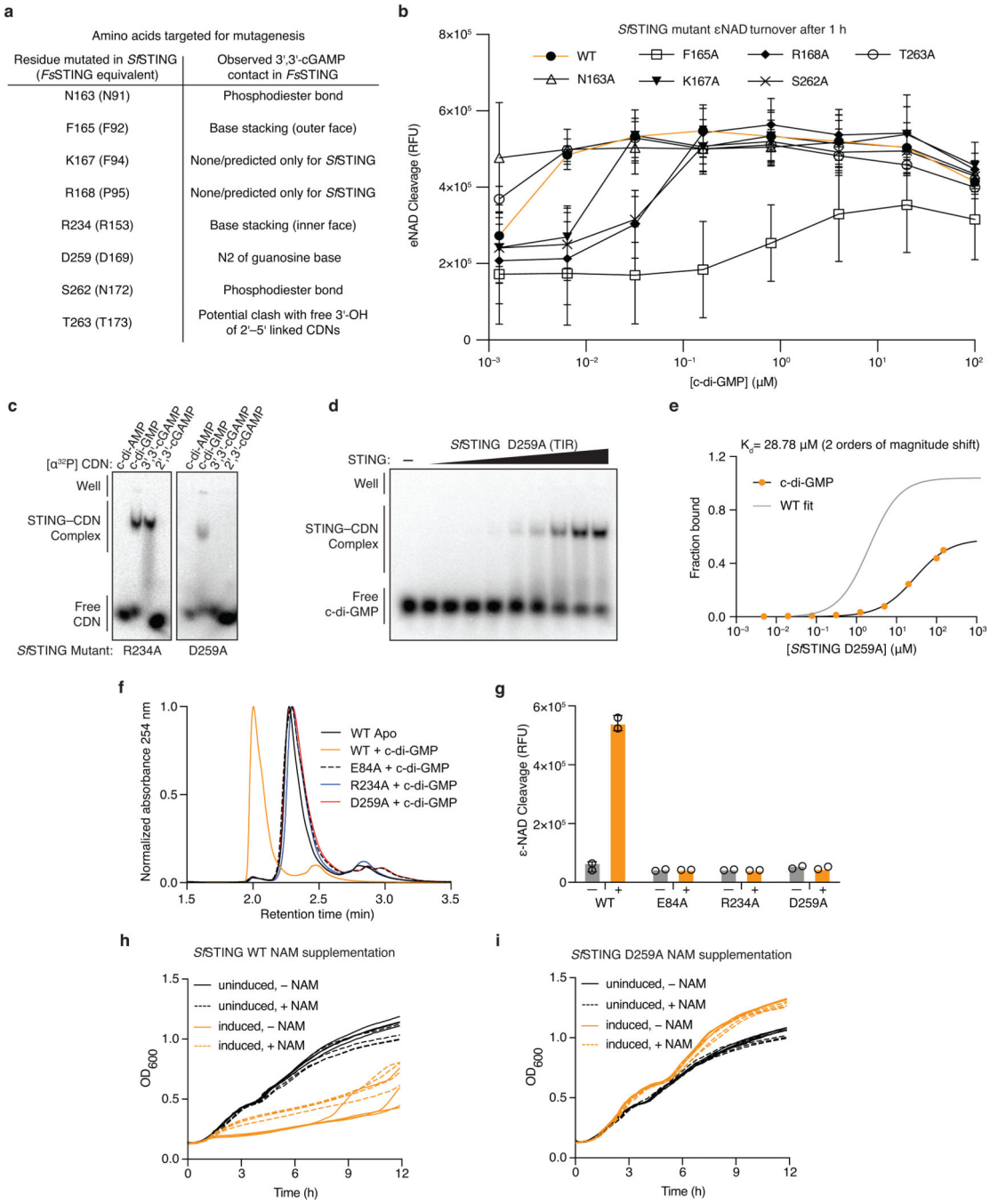

Extended Data Figure 6 |. Mutagenesis analysis of bacterial STING cyclic dinucleotide recognition and TIR activation.

a, Table of bacterial STING cyclic dinucleotide contacts tested with mutagenesis analysis. Residues were selected according to contacts observed in the structure of the *Fs*STING–3′,3′-cGAMP complex (*Fs*STING residues listed in parentheses) and tested in *Sf*STING to allow analysis of the impact on both c-di-GMP binding and NADase activity.

b, Plate reader analysis of mutant *Sf*STING NAD^+ cleavage activity in the presence of 500 nM protein and increasing c-di-GMP concentration. Mutant *Sf*STING variants with cyclic

dinucleotide binding pocket mutations require 10–1000× greater c-di-GMP concentration for NADase activation. Data are ± s.d. of n = 3 technical replicates and are representative of 3 independent experiments.

c,**d**,**e**, EMSA analysis demonstrating that *Sf*STING R234A and D259A mutations reduce stable c-di-GMP complex formation compared to *Sf*STING WT (see Figure 2d). *Sf*STING D259A protein titration and quantification confirms significantly reduced affinity for c-di-GMP. Data are representative of 3 independent experiments.

f,**g**, HPLC and plate reader analysis of mutant *Sf*STING NAD^+ cleavage activity in the presence of 500 nM protein and 10 μM c-di-GMP (HPLC) or 500 nM protein and ± 20 μM c-di-GMP (plate reader). Mutation of residues responsible for ligand recognition in the cyclic dinucleotide binding domain (R234 and D259) and catalysis in the TIR enzymatic domain (E84) disrupts *Sf*STING NADase activity and explains loss of *E. coli* toxicity observed in Figure 3d. Note, 100 μM of c-di-GMP was used for *Sf*STING D259A plate reader NAD^+ cleavage analysis to confirm complete loss of c-di-GMP-induced activation. HPLC data are representative of 3 independent experiments. Plate reader data are ± s.d. of n = 3 technical replicates and are representative of 3 independent experiments.

h,**l**, Analysis of *Sf*STING toxicity in *E. coli* cells expressing normal c-di-GMP signaling enzymes with and without nicotinamide (NAM) supplementation. NAM supplementation is sufficient to partially alleviate *Sf*STING WT-induced NADase toxicity. Each line represents the average of 2 technical replicates for each of four separately outgrown colonies. Data are representative of 2 independent experiments.

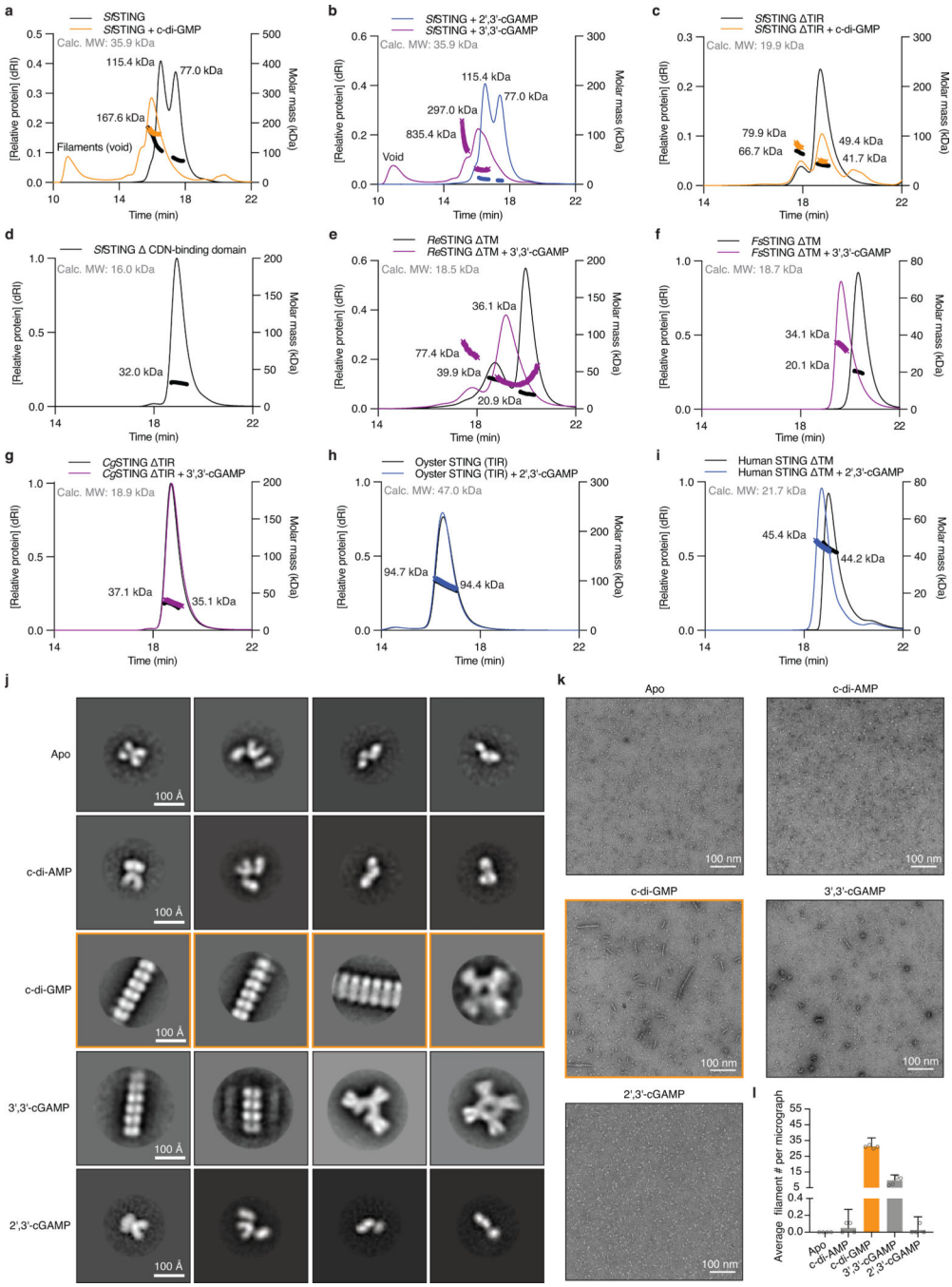

Extended Data Figure 7 |. Conservation of oligomerization as a mechanism of STING activation. **a**–**i**, STING SEC-MALS analysis. **a**,**b**, Full-length *Sf*STING changes oligomeric state in the presence of c-di-GMP or the weak agonist 3′,3′-cGAMP, and does not change oligomeric state in the presence of 2′,3′-cGAMP. **c**, With the TIR domain removed (ΔTIR), *Sf*STING no longer forms higher order complexes but notably remains dimeric in the apoprotein form. Bacterial TIR-STING proteins therefore appear to require the TIR domain to maintain stable higher-order oligomerization suggesting that intermolecular contacts are made with both TIR and STING domains. **d**, A TIR-only construct of *Sf*STING with the cyclic dinucleotide

binding domain removed (ΔCDN) elutes as a single species which is consistent with the molecular weight for a homodimer. **h**, human STING (ΔTM) is a dimer in solution with or without 2′,3′-cGAMP, confirming that TM contacts are required for oligomerization and filament formation[12,23]. Nearly all tested bacterial and metazoan STING constructs migrate as dimers in solution consistent with the cyclic dinucleotide binding domain forming a constitutive homodimeric complex for ligand recognition. Two exceptions include *Re*STING (ΔTM) and *Fs*STING (ΔTM) which form a mixture of monomeric and dimeric states in the absence of ligand and dimers or tetramers in the presence of 3′,3′-cGAMP. These results indicate that alternative oligomerization events may be required for activation of bacterial TM-STING effector function.

j, Negative stain electron microscopy 2D class averages for *Sf*STING (E84A mutant) alone or in the presence of cyclic dinucleotide ligands. Stable STING filament formation requires c-di-GMP. 2D class averages were derived from particles selected from 75 micrographs for each condition.

k, Representative micrograph images reveal extensive filament formation of varying length and orientation in the presence of c-di-GMP. Apo, c-di-AMP, and 2′,3′-cGAMP micrographs lack filaments. Images are each representative of n = 75 micrographs for each condition.

l, Particle counting analysis of micrograph images shows that c-di-GMP induces more filament formation than 3′,3′-cGAMP and stable filament formation does not occur in the presence of c-di-AMP or 2′,3′-cGAMP. Data are mean ± s.d. for quantification of n = 4 groups of 10 micrograph images each.

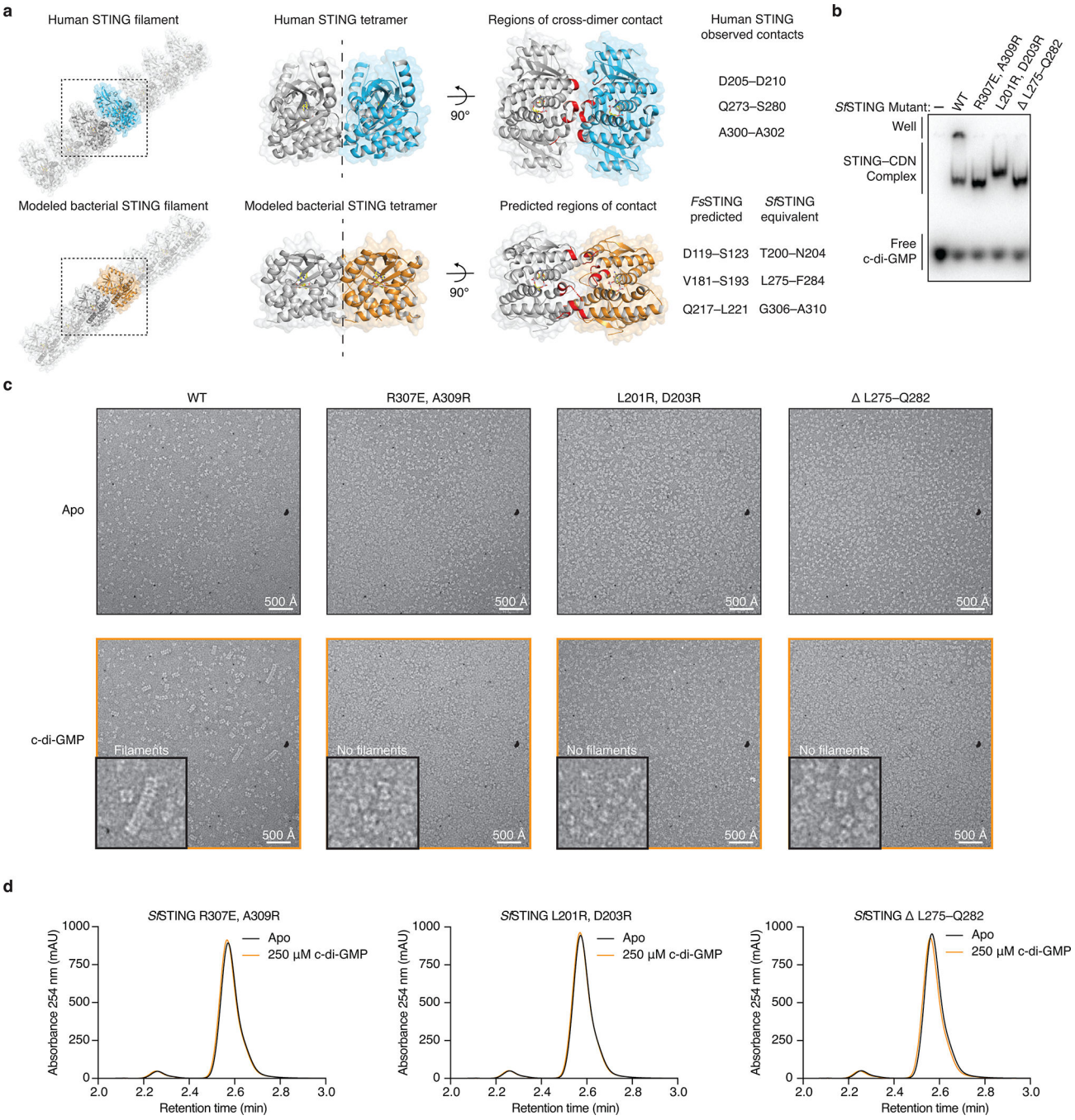

Extended Data Figure 8 |. Filament formation is required for bacterial TIR-STING activation.

a, Model of bacterial STING oligomerization and identification of surfaces involved in c-di-GMP-mediated filament formation. Electron microscopy analysis of *Sf*STING in the presence of c-di-GMP reveals filament formation likely occurs through parallel stacking of the homodimeric cyclic dinucleotide binding domain (see Extended Data Figure 7). To construct a potential model of this interaction, we used the X-ray crystal structure of the human STING–2′,3′-cGAMP complex (PDB 4KSY)[7] and the cryo-electron microscopy structure of the chicken STING tetramer (PDB 6NT8)[9] (top) as guides to position the

*Fs*STING–3′,3′-cGAMP complex structure into a tetrameric conformation. The resulting model predicts that oligomerization-mediating surfaces in *Sf*STING include T200–N204, L275–F284, and G306–A310.

b, EMSA analysis of *Sf*STING variants indicates that mutations to the predicted oligomerization surfaces do not prevent c-di-GMP recognition. *Sf*STING mutants tested include R307E/A309R, L201R/D203R, and the loop L275–Q282 replaced with a short GlySer linker (GSGGS). Data are representative of 2 independent experiments.

c, Electron microscopy analysis of *Sf*STING variants in the presence of c-di-GMP. Mutations to the *Sf*STING surfaces identified in the structural model prevent all observable cyclic dinucleotide-induced filament formation supporting their predicted role in mediating oligomerization and bacterial STING filament formation. Images are each representative of n = 5 micrographs for each condition.

d, HPLC analysis of mutant *Sf*STING NAD^+ cleavage activity in the presence of 500 nM protein and 250 μM c-di-GMP for 3 h. In the absence of cyclic dinucleotide-mediated oligomerization all *Sf*STING NADase activity is lost, confirming the requirement of filament formation in TIR domain activation. Data are representative of 3 independent experiments.

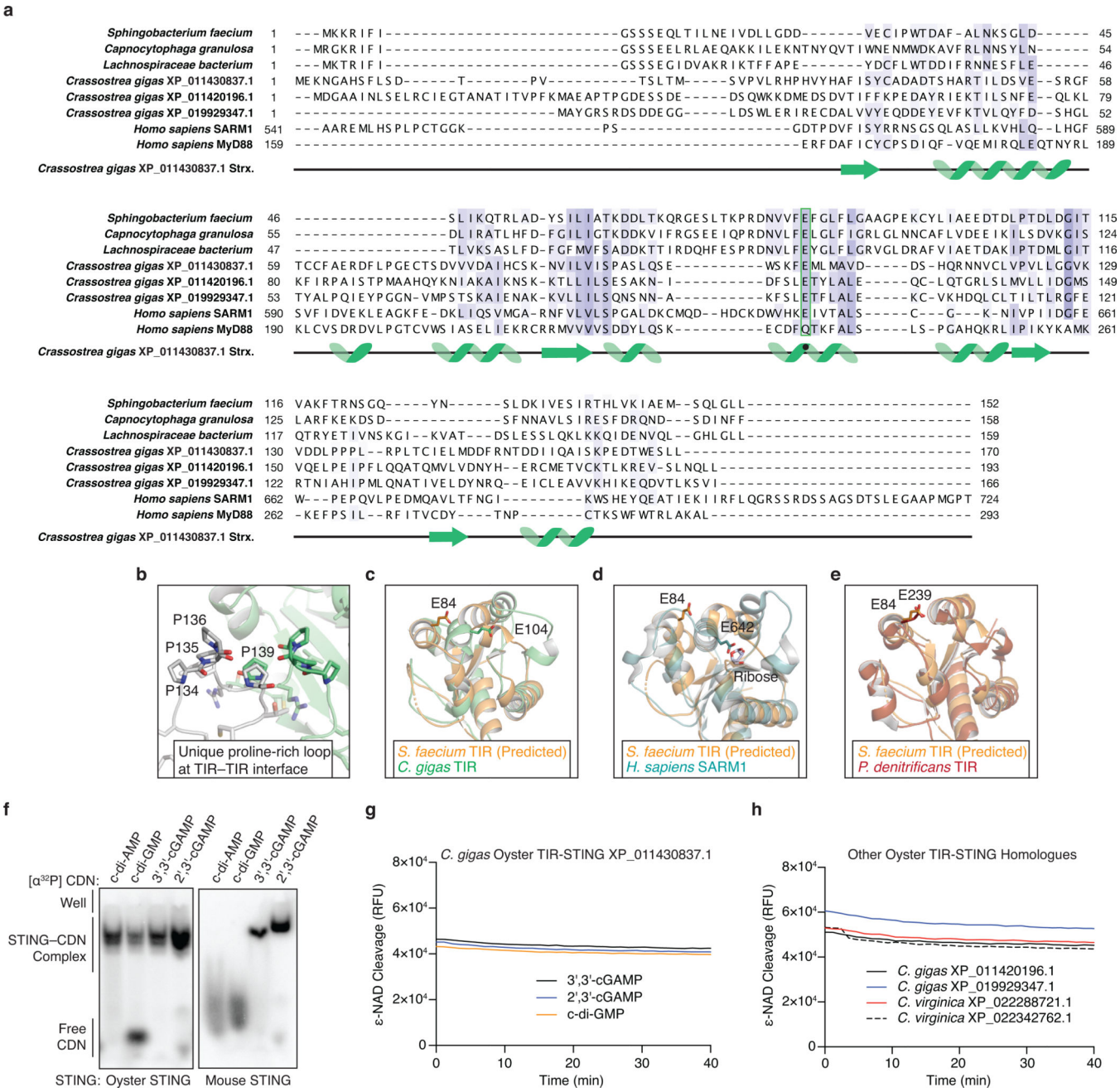

Extended Data Figure 9 |. Structural analysis of metazoan TIR-STING homologs.

a, Structure-guided alignment of the TIR domain in oyster TIR-STING with reference bacterial and metazoan TIR-domain-containing proteins. SARM1 is an example of a human TIR domain that catalyzes NAD^+ cleavage and MyD88 is an example of a human TIR domain that signals through protein–protein interaction. The catalytic glutamate responsible for supporting NAD^+ cleavage is conserved at the same spatial position among bacterial and oyster TIRs but is mutated in MyD88 (green box). However, it is not currently possible to predict from structure or sequence alone if TIR domains have enzymatic activity.

b, Distinct from other TIR domain structures, the TIR domain in oyster TIR-STING contains a proline-rich loop region at the interface suggesting a specific role in dimer stabilization.

c, Superposition of a homology model of the *Sf*STING TIR-domain with the TIR-domain of oyster TIR-STING shows the predicted catalytic glutamates for both proteins occupy distinct locations in the TIR fold.

d, Superposition of a homology model of the *Sf*STING TIR-domain compared to the crystal structure of human SARM1 bound to ribose implies that different NAD^+ binding pockets may exist between bacterial and eukaryotic TIRs as previously suggested[21].

e, Superposition of a homology model of the *Sf*STING TIR-domain with the bacterial TIR domain from *P. dentrificans* shows a high degree of similarity. No crystal structures are available for bacterial TIR domains in an active state preventing identification of a specific mechanism of catalytic activation.

f, EMSA analysis of oyster TIR-STING and mouse STING demonstrates a wide preference for cyclic dinucleotide interactions and clear ability to recognize the mammalian cGAS product 2′,3′-cGAMP. Data are representative of 3 independent experiments.

g,**h**, Oyster TIR-STING which binds all tested CDNs does not exhibit NAD^+ cleavage activity even at 10× the protein and ligand concentrations used to achieve robust activity with bacterial TIR-STING. We tested four other oyster TIR-STING homologues and observed no cyclic dinucleotide-stimulated NAD^+ cleavage activity. These results support a potential switch in TIR-dependent protein–protein interactions to control downstream signaling similar to the TIR domain in human MyD88. Data are representative of 2 independent experiments.

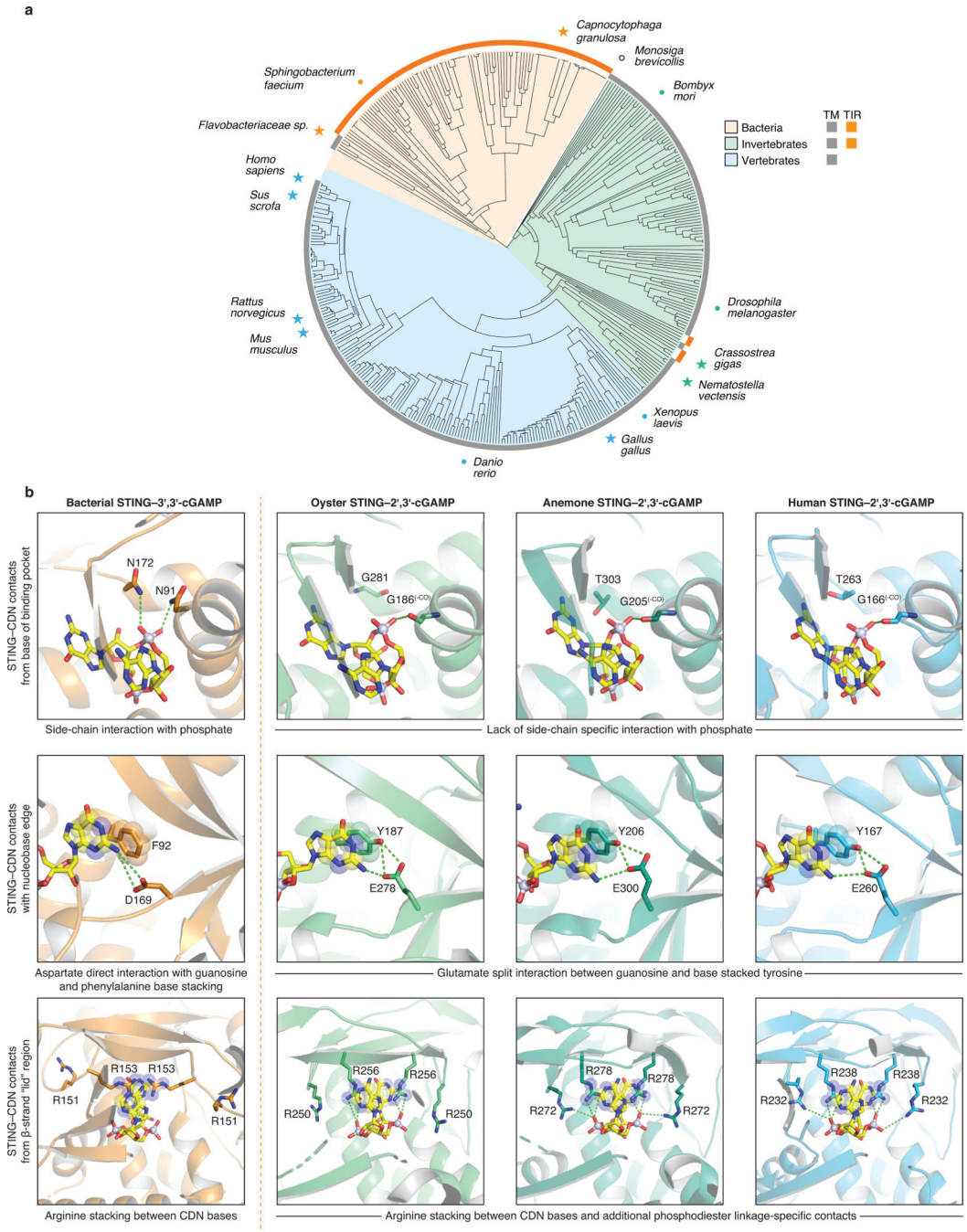

Extended Data Figure 10 |. Structure-guided analysis of STING phylogenetic conservation and cyclic dinucleotide recognition.

a, Structure-guided alignment and phylogenetic tree of STING proteins across bacterial and metazoan kingdoms. Bacterial STING homologues form a distinct cluster separate from all metazoan STING sequences and are mostly represented by TIR-STING fusions. A single STING-domain containing protein was identified in the choanoflagellate *Monosiga brevicollis* (denoted as an open black circle as this species is outside of the kingdom metazoan), no STING-domain containing proteins were found in archaea. TIR-STING fusions are rare in eukaryotes and cluster among invertebrate metazoans. No TIR-STING

examples occur in vertebrates. Specific species of interest are highlighted to show the breadth of sequence diversity and stars mark proteins with available structures. **b**, Direct comparison of bacterial, oyster, anemone, and human STING crystal structures reveals conservation of specific cyclic dinucleotide contacts and critical differences in phosphodiester linkage recognition. Stacking interactions formed with the cyclic dinucleotide nucleobase face, aromatic side chains at the top of the α-helix stem, and arginine residues extending downward from the lid region are major conserved features shared between bacterial and metazoan STING proteins. Nucleotide-specific contacts are divergent between distinct STING structures, but notably the critical D169 guanosine N2-specific contact present in bacterial STING is conserved with a glutamic acid side chain in nearly all metazoan STING proteins. A critical feature absent in bacterial STING receptors is additional arginine-specific contacts to the phosphodiester backbone. The human STING R232 side chain contact known to be critical for high-affinity interactions with 2′,3′-cGAMP is conserved throughout metazoan STINGs representing a unique adaptation not found within bacterial STING receptors. Bacterial STING–3′,3′-cGAMP (*Fs*STING), oyster STING–2′,3′-cGAMP (*C. gigas*), sea anemone STING–2′,3′-cGAMP (*N. vectensis* PDB 5CFQ)[8], human STING–2′,3′-cGAMP (*H. sapiens* PDB 4KSY)[7].

Supplementary Material

Refer to Web version on PubMed Central for supplementary material.

Acknowledgements

The authors are grateful to J. Morehouse, A. Lee, K. Chat, R. Vance, and members of the Kranzusch lab for helpful comments and discussion, Kelly Arnett and the Harvard University Center for Macromolecular Interactions, the Molecular Electron Microscopy Suite at Harvard Medical School, and the Harvard Center for Mass Spectrometry. The work was funded by the Richard and Susan Smith Family Foundation (P.J.K., S.S.), DFCI-Novartis Drug Discovery Program (P.J.K.), the Parker Institute for Cancer Immunotherapy (P.J.K.), a Cancer Research Institute CLIP Grant (P.J.K.), a V Foundation V Scholar Award (P.J.K.), the Pew Biomedical Scholars program (P.J.K.), Vallee Foundation (S.S.), the Ariane de Rothschild Women Doctoral Program (A.M.), the Israeli Council for Higher Education via the Weizmann Data Science Research Center (A.M.), the European Research Council (grant ERC-CoG 681203 to R.S.), the Ernest and Bonnie Beutler Research Program of Excellence in Genomic Medicine (R.S.), the Minerva Foundation (R.S.), the Knell Family Center for Microbiology (R.S.). B.R.M. is supported as a Ruth L. Kirschstein NRSA Postdoctoral Fellow NIH F32GM133063, A.A.G. is supported by a United States National Science Foundation Graduate Research Fellowship, B.L. is supported as a Herchel Smith Graduate Research Fellow, G.O. is supported by a Weizmann Sustainability and Energy Research Initiative (SAERI) doctoral fellowship. X-ray data were collected at the Northeastern Collaborative Access Team beamlines 24-ID-C and 24-ID-E (P30 GM124165), and used a Pilatus detector (S10RR029205), an Eiger detector (S10OD021527) and the Argonne National Laboratory Advanced Photon Source (DE-AC02–06CH11357).

References

1. Ishikawa H & Barber GN STING is an endoplasmic reticulum adaptor that facilitates innate immune signalling. Nature (2008) 455, 674–678. [PubMed: 18724357]
2. Zhong B, Yang Y, Li S, Wang YY, Li Y, Diao F, Lei C, He X, Zhang L, Tien P & Shu HB The adaptor protein MITA links virus-sensing receptors to IRF3 transcription factor activation. Immunity (2008) 29, 538–550 [PubMed: 18818105]
3. Burdette DL, Monroe KM, Sotelo-Troha K, Iwig JS, Eckert B, Hyodo M, Hayakawa Y & Vance RE STING is a direct innate immune sensor of cyclic di-GMP. Nature (2011) 478, 515–518. [PubMed: 21947006]
4. Sun L, Wu J, Du F, Chen X & Chen ZJ Cyclic GMP-AMP synthase is a cytosolic DNA sensor that activates the type I interferon pathway. Science (2013) 339, 786–791. [PubMed: 23258413]

5. Ablasser A & Chen ZJ cGAS in action: Expanding roles in immunity and inflammation. Science (2019) 363

6. Ouyang S, Song X, Wang Y, Ru H, Shaw N, Jiang Y, Niu F, Zhu Y, Qiu W, Parvatiyar K, Li Y, Zhang R, Cheng G & Liu ZJ Structural analysis of the STING adaptor protein reveals a hydrophobic dimer interface and mode of cyclic di-GMP binding. Immunity (2012) 36, 1073–1086. [PubMed: 22579474]

7. Zhang X, Shi H, Wu J, Zhang X, Sun L, Chen C & Chen ZJ Cyclic GMP-AMP containing mixed phosphodiester linkages is an endogenous high-affinity ligand for STING. Mol Cell (2013) 51, 226–235. [PubMed: 23747010]

8. Kranzusch PJ, Wilson SC, Lee AS, Berger JM, Doudna JA & Vance RE Ancient Origin of cGAS-STING Reveals Mechanism of Universal 2',3' cGAMP Signaling. Mol Cell (2015) 59, 891–903. [PubMed: 26300263]

9. Shang G, Zhang C, Chen ZJ, Bai XC & Zhang X Cryo-EM structures of STING reveal its mechanism of activation by cyclic GMP-AMP. Nature (2019) 567, 389–393. [PubMed: 30842659]

10. Cohen D, Melamed S, Millman A, Shulman G, Oppenheimer-Shaanan Y, Kacen A, Doron S, Amitai G & Sorek R Cyclic GMP-AMP signalling protects bacteria against viral infection. Nature (2019) 574, 691–695 [PubMed: 31533127]

11. Gui X, Yang H, Li T, Tan X, Shi P, Li M, Du F & Chen ZJ Autophagy induction via STING trafficking is a primordial function of the cGAS pathway. Nature (2019) 567, 262–266 [PubMed: 30842662]

12. Zhang C, Shang G, Gui X, Zhang X, Bai XC & Chen ZJ Structural basis of STING binding with and phosphorylation by TBK1. Nature (2019) 567, 394–398. [PubMed: 30842653]

13. Zhao B, Du F, Xu P, Shu C, Sankaran B, Bell SL, Liu M, Lei Y, Gao X, Fu X, Zhu F, Liu Y, Laganowsky A, Zheng X, Ji JY, West AP, Watson RO & Li P A conserved PLPLRT/SD motif of STING mediates the recruitment and activation of TBK1. Nature (2019) 569, 718–722. [PubMed: 31118511]

14. de Oliveira Mann CC, Orzalli MH, King DS, Kagan JC, Lee ASY & Kranzusch PJ Modular Architecture of the STING C-Terminal Tail Allows Interferon and NF-kappaB Signaling Adaptation. Cell Rep (2019) 27, 1165–1175 e1165 [PubMed: 31018131]

15. Whiteley AT, Eaglesham JB, de Oliveira Mann CC, Morehouse BR, Lowey B, Nieminen EA, Danilchanka O, King DS, Lee ASY, Mekalanos JJ & Kranzusch PJ Bacterial cGAS-like enzymes synthesize diverse nucleotide signals. Nature (2019) 567, 194–199. [PubMed: 30787435]

16. Ye Q, Lau RK, Mathews IT, Birkholz EA, Watrous JD, Azimi CS, Pogliano J, Jain M & Corbett KD HORMA Domain Proteins and a Trip13-like ATPase Regulate Bacterial cGAS-like Enzymes to Mediate Bacteriophage Immunity. Mol Cell (2020) 77, 709–722 e707. [PubMed: 31932165]

17. Lowey B, Whiteley AT, Keszei AFA, Morehouse BR, Mathews IT, Antine SP, Cabrera VJ, Kashin D, Niemann P, Jain M, Schwede F, Mekalanos JJ, Shao S, Lee ASY & Kranzusch PJ CBASS Immunity Uses CARF-Related Effectors to Sense 3'−5'- and 2'−5'-Linked Cyclic Oligonucleotide Signals and Protect Bacteria from Phage Infection. Cell (2020) 182, 38–49 e17 [PubMed: 32544385]

18. Jenal U, Reinders A & Lori C Cyclic di-GMP: second messenger extraordinaire. Nat Rev Microbiol (2017) 15, 271–284 [PubMed: 28163311]

19. Gao P, Ascano M, Zillinger T, Wang W, Dai P, Serganov AA, Gaffney BL, Shuman S, Jones RA, Deng L, Hartmann G, Barchet W, Tuschl T & Patel DJ Structure-function analysis of STING activation by c[G(2',5')pA(3',5')p] and targeting by antiviral DMXAA. Cell (2013) 154, 748–762. [PubMed: 23910378]

20. Essuman K, Summers DW, Sasaki Y, Mao X, Yim AKY, DiAntonio A & Milbrandt J TIR Domain Proteins Are an Ancient Family of NAD(+)-Consuming Enzymes. Curr Biol (2018) 28, 421–430 e424. [PubMed: 29395922]

21. Horsefield S et al. NAD(+) cleavage activity by animal and plant TIR domains in cell death pathways. Science (2019) 365, 793–799 [PubMed: 31439792]

22. Wan L, Essuman K, Anderson RG, Sasaki Y, Monteiro F, Chung EH, Osborne Nishimura E, DiAntonio A, Milbrandt J, Dangl JL & Nishimura MT TIR domains of plant immune receptors are

NAD(+)-cleaving enzymes that promote cell death. Science (2019) 365, 799–803. [PubMed: 31439793]

23. Ergun SL, Fernandez D, Weiss TM & Li L STING Polymer Structure Reveals Mechanisms for Activation, Hyperactivation, and Inhibition. Cell (2019) 178, 290–301 e210 [PubMed: 31230712]
24. Margolis SR, Wilson SC & Vance RE Evolutionary Origins of cGAS-STING Signaling. Trends Immunol (2017) 38, 733–743 [PubMed: 28416447]
25. Zhang G et al. The oyster genome reveals stress adaptation and complexity of shell formation. Nature (2012) 490, 49–54 [PubMed: 22992520]
26. Toshchakov VY & Neuwald AF A survey of TIR domain sequence and structure divergence. Immunogenetics (2020) 72, 181–203. [PubMed: 32002590]
27. Wexler AG & Goodman AL An insider's perspective: Bacteroides as a window into the microbiome. Nat Microbiol (2017) 2, 17026. [PubMed: 28440278]
28. Woodward JJ, Iavarone AT & Portnoy DA c-di-AMP secreted by intracellular Listeria monocytogenes activates a host type I interferon response. Science (2010) 328, 1703–1705. [PubMed: 20508090]
29. Dey B, Dey RJ, Cheung LS, Pokkali S, Guo H, Lee JH & Bishai WR A bacterial cyclic dinucleotide activates the cytosolic surveillance pathway and mediates innate resistance to tuberculosis. Nat Med (2015) 21, 401–406. [PubMed: 25730264]
30. Sixt BS, Bastidas RJ, Finethy R, Baxter RM, Carpenter VK, Kroemer G, Coers J & Valdivia RH The Chlamydia trachomatis Inclusion Membrane Protein CpoS Counteracts STING-Mediated Cellular Surveillance and Suicide Programs. Cell Host Microbe (2017) 21, 113–121. [PubMed: 28041929]
31. Loring HS, Icso JD, Nemmara VV & Thompson PR Initial Kinetic Characterization of Sterile Alpha and Toll/Interleukin Receptor Motif-Containing Protein 1. Biochemistry (2020) 59, 933–942. [PubMed: 32049506]
32. Tak U, Vlach J, Garza-Garcia A, William D, Danilchanka O, de Carvalho LPS, Saad JS & Niederweis M The tuberculosis necrotizing toxin is an NAD(+) and NADP(+) glycohydrolase with distinct enzymatic properties. J Biol Chem (2019) 294, 3024–3036. [PubMed: 30593509]
33. Ghosh J, Anderson PJ, Chandrasekaran S & Caparon MG Characterization of Streptococcus pyogenes beta-NAD+ glycohydrolase: re-evaluation of enzymatic properties associated with pathogenesis. J Biol Chem (2010) 285, 5683–5694. [PubMed: 20018886]
34. Millman A, Melamed S, Amitai G & Sorek R Diversity and classification of cyclic-oligonucleotide-based anti-phage signaling systems. Nature Microbiology (2020), 10.1038/s41564-020-0777-y.
35. Chen IA, Chu K, Palaniappan K, Pillay M, Ratner A, Huang J, Huntemann M, Varghese N, White JR, Seshadri R, Smirnova T, Kirton E, Jungbluth SP, Woyke T, Eloe-Fadrosh EA, Ivanova NN & Kyrpides NC IMG/M v.5.0: an integrated data management and comparative analysis system for microbial genomes and microbiomes. Nucleic Acids Res (2019) 47, D666–D677. [PubMed: 30289528]
36. Zhou W, Whiteley AT, de Oliveira Mann CC, Morehouse BR, Nowak RP, Fischer ES, Gray NS, Mekalanos JJ & Kranzusch PJ Structure of the Human cGAS-DNA Complex Reveals Enhanced Control of Immune Surveillance. Cell (2018) 174, 300–311 e311. [PubMed: 30007416]
37. Kabsch W Xds. Acta Crystallogr D Biol Crystallogr (2010) 66, 125–132. [PubMed: 20124692]
38. Adams PD, Afonine PV, Bunkoczi G, Chen VB, Davis IW, Echols N, Headd JJ, Hung LW, Kapral GJ, Grosse-Kunstleve RW, McCoy AJ, Moriarty NW, Oeffner R, Read RJ, Richardson DC, Richardson JS, Terwilliger TC & Zwart PH PHENIX: a comprehensive Python-based system for macromolecular structure solution. Acta Crystallogr D Biol Crystallogr (2010) 66, 213–221. [PubMed: 20124702]
39. Emsley P & Cowtan K Coot: model-building tools for molecular graphics. Acta Crystallogr D Biol Crystallogr (2004) 60, 2126–2132 [PubMed: 15572765]
40. Huang YH, Liu XY, Du XX, Jiang ZF & Su XD The structural basis for the sensing and binding of cyclic di-GMP by STING. Nat Struct Mol Biol (2012) 19, 728–730 [PubMed: 22728659]

41. Shang G, Zhu D, Li N, Zhang J, Zhu C, Lu D, Liu C, Yu Q, Zhao Y, Xu S & Gu L Crystal structures of STING protein reveal basis for recognition of cyclic di-GMP. Nat Struct Mol Biol (2012) 19, 725–727 [PubMed: 22728660]
42. Shu C, Yi G, Watts T, Kao CC & Li P Structure of STING bound to cyclic di-GMP reveals the mechanism of cyclic dinucleotide recognition by the immune system. Nat Struct Mol Biol (2012) 19, 722–724. [PubMed: 22728658]
43. Yin Q, Tian Y, Kabaleeswaran V, Jiang X, Tu D, Eck MJ, Chen ZJ & Wu H Cyclic di-GMP sensing via the innate immune signaling protein STING. Mol Cell (2012) 46, 735–745. [PubMed: 22705373]
44. Cavlar T, Deimling T, Ablasser A, Hopfner KP & Hornung V Species-specific detection of the antiviral small-molecule compound CMA by STING. EMBO J (2013) 32, 1440–1450. [PubMed: 23604073]
45. Zhang H, Han MJ, Tao J, Ye ZY, Du XX, Deng MJ, Zhang XY, Li LF, Jiang ZF & Su XD Rat and human STINGs profile similarly towards anticancer/antiviral compounds. Sci Rep (2015) 5, 18035. [PubMed: 26669264]
46. Cong X, Yuan Z, Du Y, Wu B, Lu D, Wu X, Zhang Y, Li F, Wei B, Li J, Wu J, Xu S, Wang J, Qi J, Shang G & Gu L Crystal structures of porcine STING(CBD)-CDN complexes reveal the mechanism of ligand recognition and discrimination of STING proteins. J Biol Chem (2019) 294, 11420–11432. [PubMed: 31167783]
47. Krissinel E & Henrick K Secondary-structure matching (SSM), a new tool for fast protein structure alignment in three dimensions. Acta Crystallogr D Biol Crystallogr (2004) 60, 2256–2268 [PubMed: 15572779]
48. Pei J & Grishin NV PROMALS3D: multiple protein sequence alignment enhanced with evolutionary and three-dimensional structural information. Methods Mol Biol (2014) 1079, 263–271. [PubMed: 24170408]
49. Katoh K, Rozewicki J & Yamada KD MAFFT online service: multiple sequence alignment, interactive sequence choice and visualization. Brief Bioinform (2019) 20, 1160–1166. [PubMed: 28968734]
50. Waterhouse AM, Procter JB, Martin DM, Clamp M & Barton GJ Jalview Version 2--a multiple sequence alignment editor and analysis workbench. Bioinformatics (2009) 25, 1189–1191. [PubMed: 19151095]
51. Letunic I & Bork P Interactive Tree Of Life (iTOL) v4: recent updates and new developments. Nucleic Acids Res (2019) 47, W256–W259. [PubMed: 30931475]
52. Kulasakara H, Lee V, Brencic A, Liberati N, Urbach J, Miyata S, Lee DG, Neely AN, Hyodo M, Hayakawa Y, Ausubel FM & Lory S Analysis of Pseudomonas aeruginosa diguanylate cyclases and phosphodiesterases reveals a role for bis-(3'−5')-cyclic-GMP in virulence. Proc Natl Acad Sci U S A (2006) 103, 2839–2844. [PubMed: 16477007]
53. Tang G, Peng L, Baldwin PR, Mann DS, Jiang W, Rees I & Ludtke SJ EMAN2: an extensible image processing suite for electron microscopy. J Struct Biol (2007) 157, 38–46 [PubMed: 16859925]
54. Zivanov J, Nakane T, Forsberg BO, Kimanius D, Hagen WJ, Lindahl E & Scheres SH New tools for automated high-resolution cryo-EM structure determination in RELION-3. Elife (2018) 7.
55. Zhang K Gctf: Real-time CTF determination and correction. J Struct Biol (2016) 193, 1–12. [PubMed: 26592709]
56. Kranzusch PJ, Lee ASY, Wilson SC, Solovykh MS, Vance RE, Berger JM & Doudna JA Structure-guided reprogramming of human cGAS dinucleotide linkage specificity. Cell (2014) 158, 1011–1021. [PubMed: 25131990]

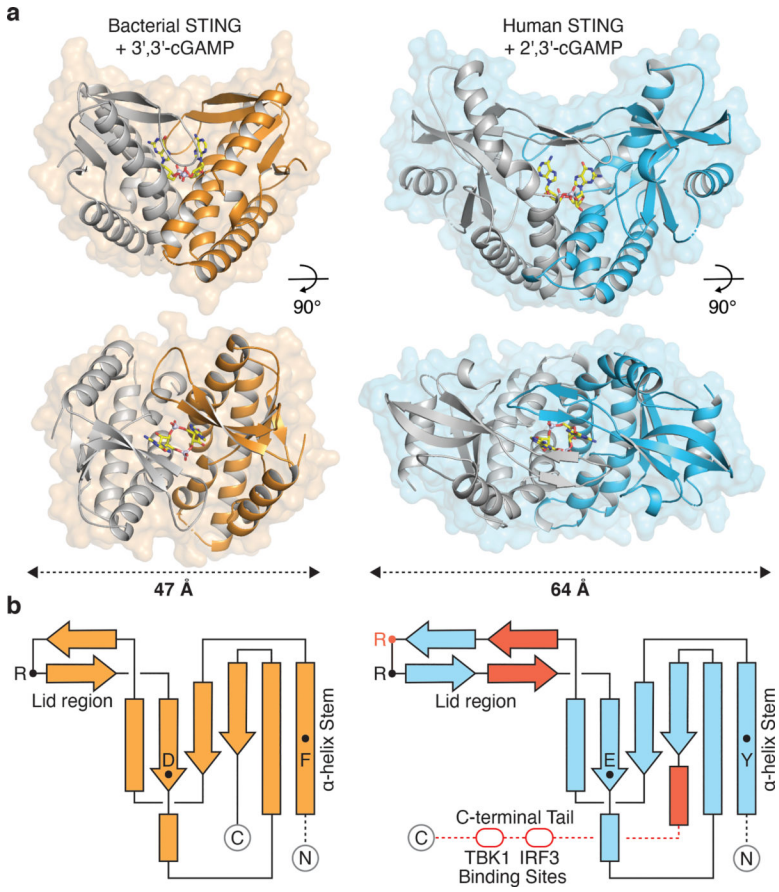

Figure 1 |. Structure of bacterial STING and definition of metazoan-specific insertions.

a, Crystal structure of a STING receptor from the bacterium *Flavobacteriaceae sp.* (orange) in complex with the cyclic dinucleotide 3′,3′-cGAMP. The *Fs*STING–3′,3′-cGAMP structure demonstrates a conserved mechanism of cyclic dinucleotide sensing shared between bacteria and human cells, and allows direct comparison with the human STING–2′,3′-cGAMP complex (PDB 4KSY, blue). For clarity, one monomer of each homodimer is depicted in grey.

b, STING topology diagrams denoting α-helices (rectangles), β-strands (arrows), and residues important for ligand recognition (*Fs*STING F92, D169, R153; hSTING Y167, E260, R232 in red, R238). Bacterial STING receptors reveal a minimal protein architecture required for cyclic dinucleotide sensing and allow direct definition of the structural insertions (red) in metazoan STING sequences required for signaling in animal cells.

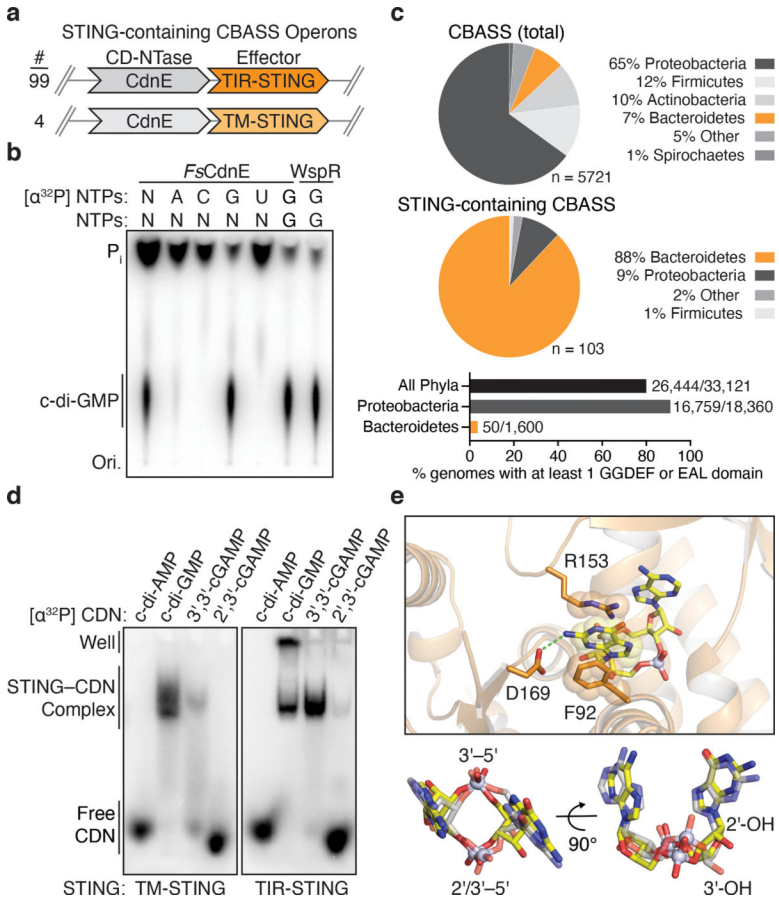

Figure 2 |. Bacterial STING systems signal through the 3′–5′-linked nucleotide second messenger c-di-GMP.

a, Schematic of STING-containing CBASS prokaryotic defense operons. STING is encoded downstream of a Clade E CD-NTase nucleotide second messenger synthase (CdnE) and exists as a fusion protein appended to Toll/Interleukin-1 receptor (TIR) or transmembrane (TM) effector modules with 99 and 4 sequences found, respectively.

b, Thin-layer chromatography analysis of *Flavobacteriaceae sp.* CdnE (*Fs*CdnE) nucleotide second messenger synthesis. CdnE enzymes in STING-containing CBASS operons require GTP for catalysis and specifically synthesize the 3′–5′-linked product c-di-GMP. Control c-di-GMP synthesis reactions performed with the GGDEF enzyme *P. aeruginosa* WspR. N, all four radiolabeled NTPs; P_i, inorganic phosphate; Ori., origin. Data are representative of 3 independent experiments.

c, Analysis of the genomic context of all STING-containing CBASS operons. STING-containing CBASS operons in bacteria are occur mainly in *Bacteroidetes* (top). Sequenced *Bacteroidetes* genomes are generally devoid of canonical GGDEF and EAL c-di-GMP signaling domains (bottom) and 97 of 99 STING-containing bacteria lack any other predicted c-di-GMP signaling component. Loss of canonical c-di-GMP signaling provides an explanation for co-option of c-di-GMP as a CD-NTase immune signal. Numbers near bar graphs denote genomes containing at least one gene with a GGDEF or EAL domain, out of total genomes in the analyzed database.

d, Electrophoretic mobility shift assay monitoring bacterial STING–cyclic dinucleotide complex formation. Bacterial TM-STING and TIR-STING proteins preferentially recognize c-di-GMP and exhibit weaker affinity for 3′,3′-cGAMP. Bacterial STING receptors are unable to recognize the mammalian second messenger 2′,3′-cGAMP. TM-STING (*R. ehrenbergii*, ΔTM) and TIR-STING (*S. faecium*, full-length). Data are representative of 3 independent experiments.

e, Zoom-in cutaway of the cyclic dinucleotide binding pocket in the *Fs*STING–3′,3′-cGAMP structure. Top, *Fs*STING makes sequence-specific contacts to the guanine base consistent with preferential c-di-GMP recognition. Bottom, bacterial STING recognizes 3′,3′-cGAMP (yellow) in a compact conformation similar to 2′,3′-cGAMP (grey) in complex with human STING (PDB 4KSY).

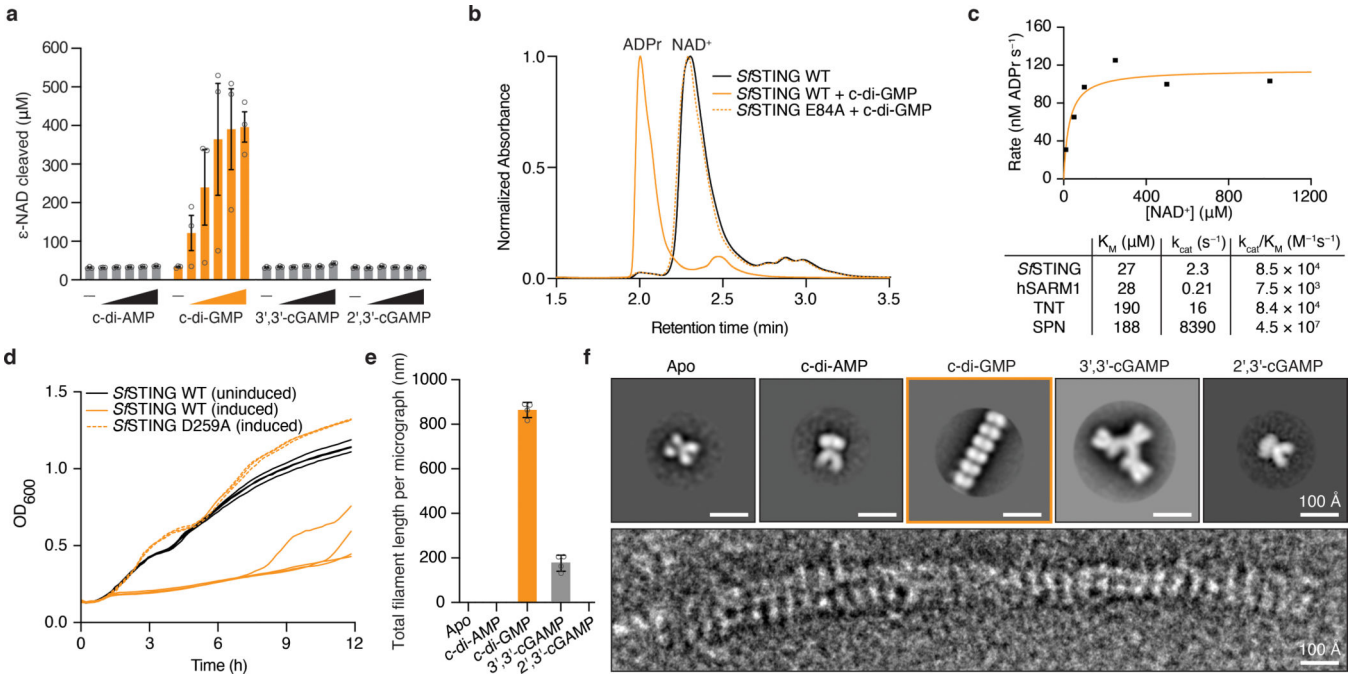

Figure 3 |. Cyclic dinucleotide-recognition controls bacterial STING oligomerization and TIR NAD$^+$ cleavage activity.

a, Analysis of *S. faecium* TIR-STING (*Sf*STING) NAD$^+$ cleavage activity using the fluorescent substrate ε-NAD. TIR-STING activity is potently stimulated in the presence of c-di-GMP (0, 5, 10, 15, 20 nM, 20 μM). Data are mean ± s.e.m. for n = 3 biological replicates.

b, HPLC analysis of TIR-STING NAD$^+$ cleavage. *Sf*STING cleaves NAD$^+$ into the products ADPr and NAM, and activity is strictly dependent on the TIR active-site residue E84. Data are representative of 3 independent experiments.

c, Quantification of *Sf*STING activity and comparison with previously characterized NADase and glycosyl hydrolase enzymes human SARM1 (hSARM1)[31], *Mycobacterium tuberculosis* TNT[32], and *Streptococcus pyogenes* SPN[33]. Data are mean for n = 2 independent replicates and are representative of 3 independent experiments.

d, Analysis of *Sf*STING toxicity in *E. coli* cells expressing normal c-di-GMP signaling enzymes. Expression of *Sf*STING from an arabinose-inducible promoter (induced) results in a potent growth arrest phenotype. Toxicity is lost with a D259A mutation to the *Sf*STING cyclic dinucleotide-binding domain that inhibits c-di-GMP recognition. Each line represents the average of 2 technical replicates for each of four separately outgrown colonies. Data are representative of 2 independent experiments.

e, Negative stain electron microscopy (EM) analysis and quantification demonstrates that *Sf*STING forms stable filaments only in the presence of c-di-GMP. Data are mean ± s.d. for quantification of n = 4 groups of 10 micrograph images.

f, Electron microscopy analysis of *Sf*STING filament formation. Top, 2D class averages demonstrate that *Sf*STING forms well-ordered filaments in the presence of c-di-GMP and smaller fragmented assemblies in the presence of 3′,3′-cGAMP. Bottom, *Sf*STING–c-di-GMP filaments can be >30 nm in length. 2D class averages were derived from particles selected from 75 micrographs for each condition.

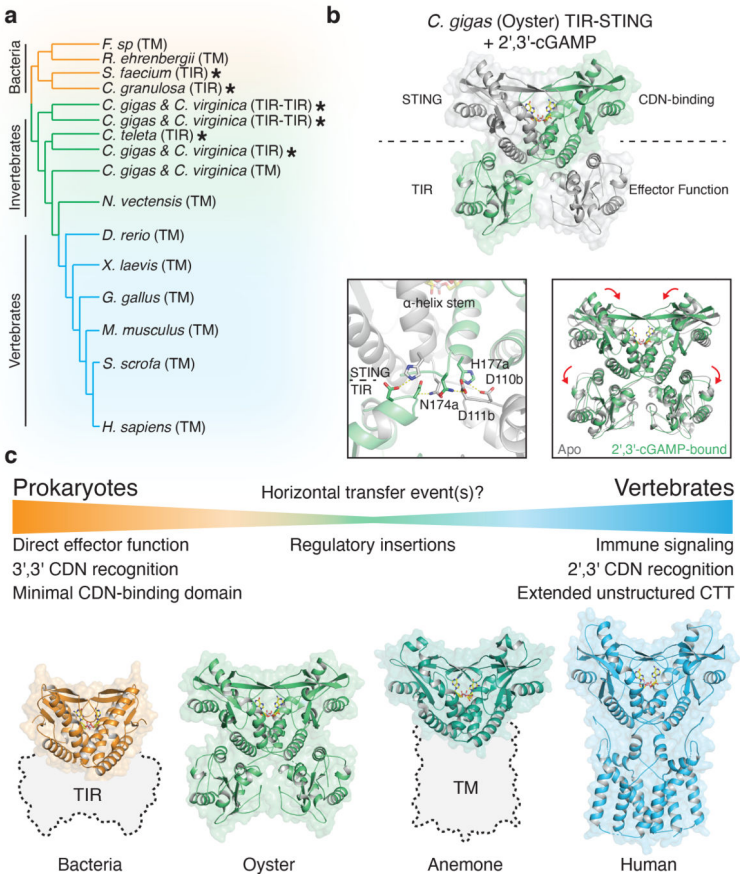

Figure 4 |. Structural basis of STING adaptation for signaling regulation.

a, Schematic derived from a structure-guided alignment of all known bacterial and metazoan STING sequences. Black stars denote TIR-STING fusions encoded in bacterial and metazoan genomes. Oysters encode several TIR-STING variants including genes predicted to contain multiple TIR domains (TIR–TIR).

b, Crystal structure of the full-length *C. gigas* (oyster) TIR-STING receptor (Genbank sequence XP_011430837.1) in complex with 2′,3′-cGAMP. Top, oyster TIR-STING adopts a domain-swapped conformation with TIR domains appended across a central dimeric axis. Bottom left, 2′,3′-cGAMP recognition results in new interactions between the STING domain α-helix stem of one monomer and the TIR domain of the other monomer. Bottom right, Ligand binding induces STING domain lid closure and a downward rotation that repositions the appended TIR domains.

c, Comparative structural analysis of STING adaptation suggests a model for the origin of cyclic dinucleotide sensing in innate immunity. STING evolved as a c-di-GMP sensor in prokaryotic bacteriophage defense, and acquisition in early metazoan cells may have allowed recognition of bacterial cyclic dinucleotides. Metazoan-specific structural insertions adapted STING for recognition of endogenous 2′,3′-cGAMP signaling and enabled antiviral and anti-tumor immune signaling in vertebrate cells. Structures shown: bacterial STING–3′,3′-cGAMP (*Fs*STING), oyster STING–2′,3′-cGAMP (*C. gigas*), sea anemone STING–

2′,3′-cGAMP (*N. vectensis* PDB 5CFQ), human STING–2′,3′-cGAMP (*H. sapiens* PDB 6NT5 modeled with 6NT7).